Postprint of: Pasika V., Nosko P., Nosko O., Bashta O., Heletiy V., Melnyk V., A method to synthesise groove cam Geneva mechanisms with increased dwell period, PROCEEDINGS OF THE INSTITUTION OF MECHANICAL ENGINEERS PART C-JOURNAL OF MECHANICAL ENGINEERING SCIENCE (2024). Copyright 2024 IMechE. DOI: 10.1177/09544062241234477

A method to synthesise groove cam Geneva mechanisms with increased dwell period

Viacheslav Pasika[a], Pavlo Nosko[b], Oleksii Nosko[c*], Oleksandr Bashta[b], Volodymyr Heletiy[a], Volodymyr Melnyk[b]

[a] Lviv Polytechnic National University,
Department of Technical Mechanics and Dynamics of Machines, Bandery 32, Lviv, 79013, Ukraine
[b] National Aviation University, Aerospace Faculty, Department of Applied Mechanics and Materials Engineering, Lubomyr Husar 1, Kyiv, 03058, Ukraine
[c] Gdansk University of Technology, Faculty of Mechanical Engineering and Ship Technology, Narutowicza 11/12, Gdansk, 80233, Poland
*Corresponding author: oleksii.nosko@pg.edu.pl, https://orcid.org/0000-0002-5259-1426

Abstract
The present study develops a method to synthesise the groove cam Geneva mechanism with increased dwell period. The main condition of the synthesis is to provide the desired law of motion of the wheel. Additional synthesis conditions are the limitation of the maximum pressure angle and the limitation of the minimum curvature radius of the cam profile. Unlike the conventional Geneva mechanisms, the synthesised groove cam Geneva mechanisms enable motion of the wheel due to an arbitrarily specified law, double locking of the wheel at its dwell-to-motion and motion-to-dwell transitions, absence of soft impacts in the extreme positions. The analysis shows that for the cycloidal law of motion, number of slots in range 3 to 15 and additional dwell coefficient in range 0 to 0.7, the operating time coefficient can be provided in wide range from 0.053 to 0.765. The effectiveness of the method is illustrated by numerical examples.

Keywords: Geneva mechanism, groove cam Geneva mechanism, synthesis method, number of wheel slots, operating time coefficient, additional dwell coefficient

Notation

a_{k}	wheel rotation invariant
b_{k}	wheel angular velocity invariant
c_{k}	wheel angular acceleration invariant
k	dimensionless time
k_{at}	additional dwell coefficient
k_{w}	operating time coefficient
l_{AB}	distance between the wheel axis and driving pin axis
l_{OA}	initial crank radius
l_{OB}	distance between the crank rotation axis and wheel axis
r	crank radius
t_{s}	wheel dwell period
t_{t}	wheel motion period
z	number of slots
λ_2	dimensionless distance between the wheel axis and driving pin axis
λ_{a}	dimensionless distance between the crank rotation axis and wheel axis
λ_{r}	dimensionless crank radius
$\lambda_{\mathrm{r1}},...,\lambda_{\mathrm{r4}}$	dimensionless crank radius in the zones I, ..., IV
λ_{rc}	dimensionless limiting radius
ν	pressure angle
$\nu_{\max}$	maximum pressure angle
$[\nu]$	allowable pressure angle
$\rho_{\min}$	dimensionless minimum curvature radius of the cam profile
$[\rho]$	dimensionless allowable curvature radius of the cam profile
φ_1	crank rotation angle
φ_2	wheel rotation angle
$\varphi_{1\Sigma}$	total crank rotation angle
$\varphi_{2\Sigma}$	total wheel rotation angle
ω_1	crank angular velocity
ω_2	wheel angular velocity
$\Delta\varphi$	additional dwell angle

1. Introduction

Increasing speeds and productivity of automatic machines require employment of highly functional and efficient cyclic mechanisms. Geneva mechanisms belong to the cyclic mechanisms commonly used in automatic machines [1–3]. Their application range is extensive and has evolved from mechanical watches and motion-picture projectors to discrete motion drives in robotic manipulators and CNC machines [4–10].

The Geneva mechanisms are simple, technological and undemanding in maintenance. However, like all lever mechanisms, they possess certain disadvantages. First of all, the laws of motion of the wheel are characterised by impact phenomena in its extreme positions, which imposes speed and energy limitations. Moreover, in the Geneva mechanism with a constant crank radius and a fixed number z of slots on the wheel, the operating time coefficient $k_{\mathrm{w}} = {}^{t_{\mathrm{t}}}/_{t_{\mathrm{s}}}$ equal to the ratio of the motion period t_{t} of the wheel to its dwell period t_{s} is governed by the number z as per the equality $k_{\mathrm{w}} = (z-2)/(z+2)$. Adjusting the coefficient k_{w} by changing the number z is not feasible in many practical cases [11].

There is a class of automatic machines and automated lines employing the Geneva mechanism where most technological operations are performed when the wheel is stationary. This class includes but is not limited to engine lathe machines, carousel lathe machines, cutting machines, milling machines, drilling machines, packaging machines, conveyor machines, lining machines. For example, if the Geneva mechanism is used in a bottle filling machine, rotation of the wheel provides placing the consecutive empty bottle under the valve, whilst filling of the bottle with liquid takes place during the dwell period t_{s}. The productivity of such automatic machines can be thus improved by reducing the motion period t_{t} or, in other words, increasing the dwell period t_{s}. However, if large inertial masses are attached to the wheel, the motion period t_{t} cannot be reduced without a significant increase in the wheel angular acceleration and, accordingly, inertial loads.

Further, the disadvantages of the Geneva mechanisms include the fact that the wheel is locked solely by a locking ring [12]. As the driving pin of the crank enters the slot, the edge of the locking ring, which is rigidly connected to the crank, comes out of contact with the wheel. High accuracy should be, therefore, guaranteed for the mutual location between the crank and locking ring. Errors in the manufacture and installation of the mechanism and its wear lead to the occurrence of unwanted gaps. This, in its turn, results in non-simultaneous entry of the driving pin into the slot and exit of the locking ring from contact, which is accompanied by increased impact loads. A similar situation is observed when the driving pin leaves the slot.

Several approaches have been proposed to improve the dynamic performance of the Geneva mechanisms. The first approach implies application of compound mechanisms to eliminate soft impacts (discontinuous accelerations) in the extreme positions [13–22]. Two or more mechanisms are connected in series so that the angular acceleration of the wheel changes continuously during its motion. This approach inevitably introduces extra components to the system. The second approach is using damping elements in the Geneva mechanism in order to reduce the impact loads [23, 24], which also leads to extra components in the system. The third approach is to modify the geometry of the slots [25–29]. Curvilinear slots are designed to provide the desired law of motion, similarly as in cam mechanisms. Although processing of the curvilinear slots is resource consuming, the approach enables adjusting the dwell period t_{s} even for a fixed number z of slots.

The study [30] investigates the applicability of the wheel with barrel-shaped slots, called ‘Quickermittent’, for motion picture film projectors. Such a mechanism allows to reduce the indexing time whilst maintaining control over the loads on the film and mechanism itself. However, due to the fact that the slot is wider in its middle part, the driving pin can hit the walls of the slot, which affects adversely on the motion stability, especially at low rotational speeds. In addition, Quickermittent mechanisms tend to be noisier than the Geneva mechanisms.

A double-pins without locking arc Geneva mechanism is developed in the study [31]. The proposed mechanism has two driving pins in contrast to the conventional Geneva mechanism with one driving pin, resulting in two times higher angular velocity of the wheel. Smaller impact loads in

the mechanism are achieved by optimising the transitional part of the slot, which implies, however, higher manufacturing costs.

The studies [2, 8, 32, 33] suggest that the functionality of the Geneva mechanism can be substantially extended by introducing a groove cam element. The groove cam Geneva mechanism comprises input crank 1, output wheel 2, groove cam 3, driving pin 4 and roller follower 5, as shown in Fig.1. The crank 1 rotates at constant angular velocity ω_1 and simultaneously moves radially due to the path of the roller follower 5 along the groove of the cam 3. The driving pin 4 on the crank 1 brings the wheel 2 in motion. Thus, the mechanism makes use of the cam 3 to control the radius of action of the driving pin 4, which provides the necessary kinematic characteristics of the wheel 2.

[insert Figure 1.]

The analysis of the above-mentioned studies indicates a lack of research devoted to solving the problem of synthesising the groove cam Geneva mechanism and analysing the influence of different parameters on its performance. The purpose of the present study is to develop a method to synthesise the groove cam Geneva mechanism with increased dwell period that satisfies the desired law of motion of the wheel (main condition), allowable pressure angle and allowable curvature radius of the cam profile (additional conditions). The following tasks are solved to achieve this purpose: development of the general approach to determining the path of the driving pin due to the specified operating time coefficient k_{w} (Section 2); formulation of the additional conditions of synthesis (Section 3); development of the method to synthesise the driving pin path (Section 4); development of the synthesis algorithm (Section 5); illustration of the method application (Section 6).

2. General approach to determining the driving pin path

A detailed schematic of the groove cam Geneva mechanism is shown in Fig.2. The numbering of the elements in the schematic corresponds to Fig.1. In addition to the input crank 1, output wheel 2, groove cam 3, driving pin 4 and roller follower 5, Fig.2 presents the locking ring 6. To reduce the number of parameters in the present study and simplify analysis, the roller follower 5 is assumed to have a common axis with the driving pin 4, i.e. the centre C of the roller follower 5 coincides with the centre A of the driving pin 4. Under this assumption, the profile of the cam 3 coincides with the path of the centre A of the driving pin 4.

[insert Figure 2.]

Imagine that the driving pin 4 enters the slot of the wheel 2 at the moment when the crank 1 and slot are mutually perpendicular. The driving pin 4 passes then along the slot from the position A to the position A_1, which corresponds to a certain rotation angle $\Delta\varphi$ of the crank 1. In this interval, the wheel 2 is stationary due to its locking by the ring 6 and motion of the driving pin 4 along the line AA_1. As the crank 1 rotates by the angle $\Delta\varphi$, the wheel 2 is brought in motion. Apparently, the described situation corresponds to an increase in the dwell period t_{s} of the wheel 2. The angle $\Delta\varphi$ is referred to as 'additional dwell angle'.

There is thus a principal difference between the operation of the conventional Geneva mechanism and that of the groove cam Geneva mechanism. In the former, the locking of the wheel at its dwell-to-motion and motion-to-dwell transitions is performed solely by the locking ring, whereas in the latter it is performed by both locking ring 6 and driving pin 4.

Derive an analytical expression for the operating time coefficient k_{w}. Introduce the total crank rotation angle $\varphi_{1\Sigma}$ and total wheel rotation angle $\varphi_{2\Sigma}$ as

$$\varphi_{1\Sigma} = \pi\left(1 - \frac{2}{z}\right);$$

$$\varphi_{2\Sigma} = \frac{2\pi}{z}$$

Further, express the motion period t_t and dwell period t_s in the form

$$t_t = \frac{\varphi_{1\Sigma} - 2\Delta\varphi}{\omega_1};$$

$$t_s = \frac{2\pi - \varphi_{1\Sigma} + 2\Delta\varphi}{\omega_1}$$

Based on the equations above, the operating time coefficient k_w can be expressed as follows:

$$k_w = \frac{t_t}{t_s} = \frac{\pi(z-2)/z - 2\Delta\varphi}{\pi(z+2)/z + 2\Delta\varphi} \quad (1)$$

After defining the additional dwell coefficient as the ratio

$$k_{at} = \frac{2\Delta\varphi}{\varphi_{1\Sigma}}$$

Eq.(1) can be rewritten in the following manner:

$$k_w = \frac{(z-2)(1-k_{at})}{2z - (z-2)(1-k_{at})} \quad (2)$$

Apparently, the operating time coefficient k_w is reduced at $\Delta\varphi > 0$ and, accordingly, $k_{at} > 0$. As the coefficient k_{at} tends to 1, the additional dwell angle $\Delta\varphi$ increases significantly along with the geometric dimensions of the mechanism (see Fig.2). It is reasonable, therefore, to limit k_{at}, and the present study accepts that $k_{at} \leq 0.7$. Due to the fact that the number z of slots cannot be less than 3, whilst the Geneva mechanisms with $z > 15$ are rarely met in practice, the number z is accepted to be in range from 3 to 15.

Fig.3 illustrates the dependence of the operating time coefficient k_w on the additional dwell coefficient k_{at} and number z due to Eq.(2). The analysis shows that for the conventional Geneva mechanism ($k_{at} = 0$), the coefficient k_w changes from 0.2 to 0.765. By contrast, the groove cam Geneva mechanism has a significantly wider range of the coefficient k_w from 0.053 to 0.765 at $0 < k_{at} \leq 0.7$. Note that the coefficient k_w is more sensitive to the variation of k_{at} at smaller values of k_{at}.

[insert Figure 3.]

Considering Fig.2, introduce the dimensionless crank radius λ_r, dimensionless distance λ_2 between the driving pin axis A and wheel axis B, dimensionless distance λ_a between the crank rotation axis O and wheel axis B as

$$\lambda_r = \frac{r}{l_{OA}};$$

$$\lambda_2 = \frac{l_{AB}}{l_{OA}};$$

$$\lambda_a = \frac{l_{OB}}{l_{OA}} = \frac{1}{\sin(\pi/z)}$$

where r is the crank radius, i.e. the distance between the crank rotation axis O and driving pin axis A; l_{AB} is the distance between the driving pin axis A and wheel axis B; l_{OB} is the distance between the crank rotation axis O and wheel axis B; l_{OA} is the initial crank radius for the perpendicular position between the crank and slot.

Writing the equation of closed vector circuit in the form

$$\bar{\lambda}_{\mathrm{r}} + \bar{\lambda}_2 = \bar{\lambda}_{\mathrm{a}}$$

and projecting it on the horizontal and vertical axes yield that

$$\lambda_{\mathrm{r}} = \lambda_{\mathrm{a}} \frac{\sin\left(\pi/z - \varphi_2\right)}{\cos\left(\varphi_1 + \varphi_2\right)};$$

$$\lambda_2 = \lambda_{\mathrm{a}} \frac{\cos\left(\pi/z + \varphi_1\right)}{\cos\left(\varphi_1 + \varphi_2\right)} \tag{3}$$

where φ_1 and φ_2 are the rotation angles of the respective crank and wheel.

Further, represent the rotation angles of the respective crank and wheel in the form

$$\varphi_1 = k\varphi_{1\Sigma};$$

$$\varphi_2 = a_{\mathrm{k}}\varphi_{2\Sigma}$$

where $k = \varphi_1/\varphi_{1\Sigma}$ is the dimensionless time; a_{k} is the wheel rotation invariant. Then the derivatives of the radius λ_{r} with respect to φ_1 read

$$\lambda'_{\mathrm{r}} = \frac{d\lambda_{\mathrm{r}}}{d\varphi_1} = \frac{\lambda_{\mathrm{a}}}{\cos^2\left(\varphi_1 + \varphi_2\right)}\left(\sin\left(\varphi_1 + \varphi_2\right)\sin\left(\frac{\pi}{z} - \varphi_2\right) - \varphi'_2\cos\left(\frac{\pi}{z} + \varphi_1\right)\right);$$

$$\lambda''_{\mathrm{r}} = \frac{d^2\lambda_{\mathrm{r}}}{d\varphi_1^2} = -\frac{\lambda_{\mathrm{a}}}{\cos^3\left(\varphi_1 + \varphi_2\right)}\left(\varphi''_2\cos\left(\varphi_1 + \varphi_2\right)\cos\left(\frac{\pi}{z} + \varphi_1\right) + 2\varphi'_2\right.$$
$$\left(\left(1 + \varphi'_2\right)\cos\left(\varphi_1 + \varphi_2\right)\sin\left(\frac{\pi}{z} + \varphi_1\right) - \left(2 + \varphi'_2\right)\sin\left(\frac{\pi}{z} - \varphi_2\right)\right)$$
$$\left. + \left(1 + \sin^2\left(\varphi_1 + \varphi_2\right)\right)\sin\left(\frac{\pi}{z} - \varphi_2\right)\right) \tag{4}$$

with

$$\varphi'_2 = \frac{d\varphi_2}{d\varphi_1} = b_{\mathrm{k}}\frac{\varphi_{2\Sigma}}{\varphi_{1\Sigma}};$$

$$\varphi''_2 = \frac{d^2\varphi_2}{d\varphi_1^2} = c_{\mathrm{k}}\frac{\varphi_{2\Sigma}}{\varphi_{1\Sigma}^2} \tag{5}$$

where $b_{\mathrm{k}} = da_{\mathrm{k}}/dk$ and $c_{\mathrm{k}} = db_{\mathrm{k}}/dk$ are the wheel angular velocity and acceleration invariants.

Thus, as the crank radius λ_{r} changes due to Eq.(3), the wheel moves according to the prescribed law with rotation invariant a_{k}. Remember that the expressions for λ_{r}, λ'_{r}, λ''_{r} given by Eqs.(3)–(5) are valid if the wheel motion starts from the perpendicular position between the crank and slot.

3. Additional conditions of synthesis

Since the studied mechanism (see Fig.2) includes a cam mechanism in the form of the roller follower in contact with the groove cam, the additional conditions of synthesis arise, as considered next.

3.1. Limitation condition for the maximum pressure angle

In order to prevent jamming in the cam mechanism, the maximum value $\nu_{\max}$ of the pressure angle

$$\nu = \arctan\frac{\lambda_{\mathrm{r}}'}{\lambda_{\mathrm{r}}} \tag{6}$$

should not exceed the allowable pressure angle $[\nu]$. The corresponding condition limiting the maximum pressure angle $\nu_{\max}$ is formulated as

$$\nu_{\max} \leq [\nu] \tag{7}$$

The allowable pressure angle $[\nu]$ is chosen depending on the angular velocity and load in the cam mechanism. In most engineering applications, the value of $[\nu]$ is in range from 30° to 45°. In the present study, $[\nu]$ is accepted to be between 32.5° and 41.6°, which corresponds to the case of rotary tables like Vertex Precision Tilting Rotary Table VUT used in carousel lathe machines, cutting machines, milling machines, drilling machines and conveyor machines [33].

3.2. Limitation condition for the minimum curvature radius of the cam profile

In order to prevent sharpening and interference of the cam profile, it is necessary to limit from below its minimum curvature radius $\rho_{\min}$. The allowable curvature radius $[\rho]$ of the cam profile is determined by the dimensionless expression [34]

$$[\rho] = \max\left\{\frac{\lambda_{\mathrm{r}}'}{\tan[\nu]} - \lambda_{\mathrm{r}} + \min\lambda_{\mathrm{r}}\right\} \tag{8}$$

The minimum curvature radius $\rho_{\min}$ of the cam profile is derived from the known formula for the radius of curvature given in polar coordinates as

$$\rho_{\min} = \min\left\{\frac{\left(\lambda_{\mathrm{r}}^2 + \left(\lambda_{\mathrm{r}}'\right)^2\right)^{3/2}}{\lambda_{\mathrm{r}}^2 + 2\left(\lambda_{\mathrm{r}}'\right)^2 - \lambda_{\mathrm{r}}\lambda_{\mathrm{r}}''}\right\} \tag{9}$$

The condition limiting the minimum curvature radius $\rho_{\min}$ takes then the following form:

$$\rho_{\min} \geq [\rho] \tag{10}$$

Thus, the additional conditions of synthesis include Eq.(7) limiting the maximum pressure angle $\nu_{\max}$ and Eq.(10) limiting the minimum curvature radius $\rho_{\min}$ of the cam profile.

4. Method to synthesise the driving pin path

Fig.4 shows the characteristic zones of the crank motion: I — linear path of the driving pin, stationary wheel; II — path of the driving pin for the wheel motion period; III — linear path of the driving pin, stationary wheel; IV — path of the driving pin which provides a smooth conjugation of the end of the zone III and the start of the zone I. The crank radius λ_{r} is determined next for each zone.

[insert Figure 4.]

Zone I starts in the position A when the driving pin enters the slot, and it ends in the position A_1 when the crank rotates by the additional dwell angle $\Delta\varphi$. The rotation angle φ_1 of the crank

changes, thereby, from 0 to $\Delta\varphi$. Considering the fact that the wheel is stationary, i.e. $\varphi_2 = 0$, a simplified expression for the crank radius λ_{r1} is derived in the form

$$\lambda_{r1} = \frac{1}{\cos\varphi_1} \tag{11}$$

Zone II starts in the position A_1 and ends in the position A_1'. The wheel moves according to the prescribed law. The crank rotation angle φ_1 changes from $\Delta\varphi$ to $(\varphi_{1\Sigma} - \Delta\varphi)$. The crank radius λ_{r2} is found from Eqs.(3)–(5).

Zone III starts in the position A_1' and ends in the position A'. The motion of the driving pin occurs similarly to that in the zone I. The crank rotation angle φ_1 changes from $(\varphi_{1\Sigma} - \Delta\varphi)$ to $\varphi_{1\Sigma}$. Since $\varphi_2 = \varphi_{2\Sigma} = 2\pi/z$, the expression for the crank radius λ_{r3} reads

$$\lambda_{r3} = -\frac{1}{\cos\left(2\pi/z + \varphi_1\right)}$$

Zone IV starts in the position A' and ends in the position A. Accordingly, the crank rotation angle φ_1 changes from $\varphi_{1\Sigma}$ to 2π. The crank radius λ_{r4} can be defined in the form of polynomial

$$\lambda_{r4} = \sum_{i=1}^{n} a_i \varphi_1^{i-1} \tag{12}$$

where n is the number of the conditions imposed on the crank radius λ_{r4}.

The boundary conditions are formulated to prevent soft impacts at the start of the zone I in the position A and at the end of the zone III in the position A'. This can be achieved by smooth conjugation of the crank radius and its first three derivatives, i.e.

$$\begin{aligned}
\lambda_{r4} &= \lambda_{r3}\big|_{\varphi_1 = \varphi_{1\Sigma}};\\
\lambda_{r4}' &= \lambda_{r3}'\big|_{\varphi_1 = \varphi_{1\Sigma}};\\
\lambda_{r4}'' &= \lambda_{r3}''\big|_{\varphi_1 = \varphi_{1\Sigma}};\\
\lambda_{r4}''' &= \lambda_{r3}'''\big|_{\varphi_1 = \varphi_{1\Sigma}}
\end{aligned} \tag{13}$$

and

$$\begin{aligned}
\lambda_{r4}\big|_{\varphi_1 = 2\pi} &= \lambda_{r1}\big|_{\varphi_1 = 0};\\
\lambda_{r4}'\big|_{\varphi_1 = 2\pi} &= \lambda_{r1}'\big|_{\varphi_1 = 0};\\
\lambda_{r4}''\big|_{\varphi_1 = 2\pi} &= \lambda_{r1}''\big|_{\varphi_1 = 0};\\
\lambda_{r4}'''\big|_{\varphi_1 = 2\pi} &= \lambda_{r1}'''\big|_{\varphi_1 = 0}
\end{aligned} \tag{14}$$

Since there is infinite number of functions satisfying Eq.(13) and Eq.(14), additional conditions should be formulated. In the bisector of the zone IV, which corresponds to the crank rotation angle $\varphi_1 = \varphi_c = \varphi_{1\Sigma}/2 + \pi$, the crank radius λ_{r4} is set equal to the dimensionless limiting radius λ_{rc}, i.e.

$$\lambda_{r4}\big|_{\varphi_1 = \varphi_c} = \lambda_{rc} \tag{15}$$

and the rate of change of λ_{r4} is set equal to zero, i.e.

$$\lambda_{r4}'\big|_{\varphi_1 = \varphi_c} = 0 \tag{16}$$

Thereby, the total number of the conditions given by Eqs.(13)–(16) equals $n = 10$. These conditions lead to the following system of equations with respect to the coefficients a_i in Eq.(12):

$$\begin{pmatrix} 1 & \varphi_{1\Sigma} & \varphi_{1\Sigma}^2 & \varphi_{1\Sigma}^3 & \varphi_{1\Sigma}^4 & \varphi_{1\Sigma}^5 & \varphi_{1\Sigma}^6 & \varphi_{1\Sigma}^7 & \varphi_{1\Sigma}^8 & \varphi_{1\Sigma}^9 \\ 0 & 1 & 2\varphi_{1\Sigma} & 3\varphi_{1\Sigma}^2 & 4\varphi_{1\Sigma}^3 & 5\varphi_{1\Sigma}^4 & 6\varphi_{1\Sigma}^5 & 7\varphi_{1\Sigma}^6 & 8\varphi_{1\Sigma}^7 & 9\varphi_{1\Sigma}^8 \\ 0 & 0 & 2 & 6\varphi_{1\Sigma} & 12\varphi_{1\Sigma}^2 & 20\varphi_{1\Sigma}^3 & 30\varphi_{1\Sigma}^4 & 42\varphi_{1\Sigma}^5 & 56\varphi_{1\Sigma}^6 & 72\varphi_{1\Sigma}^7 \\ 0 & 0 & 0 & 6 & 24\varphi_{1\Sigma} & 60\varphi_{1\Sigma}^2 & 120\varphi_{1\Sigma}^3 & 210\varphi_{1\Sigma}^4 & 336\varphi_{1\Sigma}^5 & 504\varphi_{1\Sigma}^6 \\ 1 & \varphi_e & \varphi_e^2 & \varphi_e^3 & \varphi_e^4 & \varphi_e^5 & \varphi_e^6 & \varphi_e^7 & \varphi_e^8 & \varphi_e^9 \\ 0 & 1 & 2\varphi_e & 3\varphi_e^2 & 4\varphi_e^3 & 5\varphi_e^4 & 6\varphi_e^5 & 7\varphi_e^6 & 8\varphi_e^7 & 9\varphi_e^8 \\ 0 & 0 & 2 & 6\varphi_e & 12\varphi_e^2 & 20\varphi_e^3 & 30\varphi_e^4 & 42\varphi_e^5 & 56\varphi_e^6 & 72\varphi_e^7 \\ 0 & 0 & 0 & 6 & 24\varphi_e & 60\varphi_e^2 & 120\varphi_e^3 & 210\varphi_e^4 & 336\varphi_e^5 & 504\varphi_e^6 \\ 1 & \varphi_c & \varphi_c^2 & \varphi_c^3 & \varphi_c^4 & \varphi_c^5 & \varphi_c^6 & \varphi_c^7 & \varphi_c^8 & \varphi_c^9 \\ 0 & 1 & 2\varphi_c & 3\varphi_c^2 & 4\varphi_c^3 & 5\varphi_c^4 & 6\varphi_c^5 & 7\varphi_c^6 & 8\varphi_c^7 & 9\varphi_c^8 \end{pmatrix} \begin{pmatrix} a_1 \\ a_2 \\ a_3 \\ a_4 \\ a_5 \\ a_6 \\ a_7 \\ a_8 \\ a_9 \\ a_{10} \end{pmatrix} = \begin{pmatrix} \lambda_{r3}|_{\varphi_{1\Sigma}} \\ \lambda'_{r3}|_{\varphi_{1\Sigma}} \\ \lambda''_{r3}|_{\varphi_{1\Sigma}} \\ \lambda'''_{r3}|_{\varphi_{1\Sigma}} \\ \lambda_{r1}|_0 \\ \lambda'_{r1}|_0 \\ \lambda''_{r1}|_0 \\ \lambda'''_{r1}|_0 \\ \lambda_{rc} \\ 0 \end{pmatrix} \tag{17}$$

where φ_e stands for 2π for shorter notation.

Now it is turn to determine the maximum pressure angle ν_{max} and minimum curvature radius ρ_{min} of the cam profile for each zone and compare them to the allowable values $[\nu]$ and $[\rho]$, respectively.

4.1. Limitation condition for the maximum pressure angle

Zone I. Substitution of Eq.(11) into Eq.(6) results in the pressure angle $\nu = \varphi_1$. Since the crank rotation angle φ_1 changes from 0 to $\Delta\varphi$, it is true that the maximum pressure angle equals $\nu_{max} = \Delta\varphi$. The condition of Eq.(7) is thus fulfilled if $\Delta\varphi \le [\nu]$ or, taking account of Eq.(1) and Eq.(2), if

$$k_{at} \le \frac{2z}{\pi(z-2)}[\nu] \tag{18}$$

Fig.5a shows the range of the additional dwell coefficient k_{at} that satisfies Eq.(18). The coefficient k_{at} can take any value between 0 and 0.7 for $z \in \{3,4\}$. As the number z of slots increases, the upper limit of the range decreases. For $z = 15$, it equals 0.417 at $[\nu] = 32.5°$ and 0.532 at $[\nu] = 41.6°$

[insert Figure 5.]

Zone II. Substitution of Eq.(3) and Eq.(4) into Eq.(6) allows deriving the expression of the pressure angle ν in the form

$$\tan\nu = \frac{\sin(\varphi_1+\varphi_2)\sin(\pi/z-\varphi_2) - \varphi_2'\cos(\pi/z+\varphi_1)}{\cos(\varphi_1+\varphi_2)\sin(\pi/z-\varphi_2)} \tag{19}$$

Assume that the wheel moves according to the cycloidal law

$$a_k = k - \frac{\sin(2\pi k)}{2\pi} \tag{20}$$

which is widespread in the cyclic mechanisms, providing zero angular acceleration of the wheel in its extreme positions, i.e. at the start and end of its motion period.

The maximum pressure angle ν_{max} is determined based on Eq.(19) and Eq.(20). Fig.5b shows the corresponding range of the coefficient k_{at} satisfying Eq.(7). As in the case of zone I, the coefficient k_{at} can be arbitrary from 0 to 0.7 for $z \in \{3,4\}$. As the number z increases, the upper

limit of the range decreases. For $z = 15$, it equals 0.375 at $[\nu] = 32.5°$ and 0.506 at $[\nu] = 41.6°$. Comparison of Fig.5a and Fig.5b shows that the coefficient k_{at} is smaller in the zone II for any z.

Zone III. Since the zones I and III are symmetrical about the vertical axis (see Fig.4), similar conclusions can be drawn here as for the zone I.

Zone IV. The crank radius λ_{r4} represents the polynomial of Eq.(12) with the coefficients a_i satisfying Eq.(17). The dependence of the maximum pressure angle ν_{max} on the number z and limiting radius λ_{rc} is obtained based on Eq.(6). Fig.6 shows the relevant data for the limiting radius λ_{rc} that changes from 1 to 2.2 with step 0.2. It is seen that for $[\nu] = 32.5°$, the condition of Eq.(7) is fulfilled at $1 \le \lambda_{rc} \le 2$ and any z, as well as at $\lambda_{rc} = 2.2$ and $z \le 7$. For $[\nu] = 41.6°$, the entire range of λ_{rc} satisfies the condition of Eq.(7). Note that the maximum pressure angle ν_{max} increases with increasing λ_{rc}.

[insert Figure 6.]

Summarising the results for all zones leads to the conclusion that the condition of Eq.(7) limiting the maximum pressure angle ν_{max} can be fulfilled for any z. As the number z increases, the upper limit of the coefficient k_{at} decreases. For $[\nu] = 32.5°$, it equals 0.7 at $z = 3$ and 0.375 at $z = 15$, whilst for $[\nu] = 41.6°$, it is about 1.3 times larger. The coefficient k_{at} should be chosen according to the results obtained for the zone II (see Fig.5b). Additionally, the limiting radius λ_{rc} should be specified as small as possible to reduce the maximum pressure angle ν_{max}.

4.2. Limitation condition of the minimum curvature radius of the cam profile

Zone I. Since the path AA_1 of the driving pin is linear (see Fig.4), the curvature radius of the cam profile is infinitely large.

Zone II. Substitution of Eq.(20) into Eqs.(3)–(5) allows determining the allowable curvature radius $[\rho]$ of the cam profile due to Eq.(8) and the minimum curvature radius ρ_{min} of the cam profile due to Eq.(9). Fig.7 shows the range of the coefficient k_{at} satisfying the condition of Eq.(10) in dependence on the number z. The analysis reveals that for $[\nu] = 32.5°$, the synthesis of the driving pin path is possible at $z \ge 4$. The coefficient k_{at} is in range from 0 to 0.29 at $4 \le z \le 13$ and in range from 0 to 0.28 at $z \in \{14,15\}$. As for $[\nu] = 41.6°$, the condition of Eq.(10) is fulfilled for any z. The upper limit of the coefficient k_{at} equals 0.34 at $z = 3$, 0.37 at $z \in \{4,5,6,13,14,15\}$ and 0.38 at $7 \le z \le 12$.

[insert Figure 7.]

Zone III. Similar conclusions are valid as for the zone I due to the symmetry of the zones I and III about the vertical axis (see Fig.4).

Zone IV. The crank radius λ_{r4} is described by the polynomial Eq.(12) with the coefficients a_i satisfying Eq.(17). Fig.8 shows the allowable curvature radius $[\rho]$ of the cam profile determined based on Eq.(8). Fig.9 shows the minimum curvature radius ρ_{min} of the cam profile determined by Eq.(9).

[insert Figure 8.]

[insert Figure 9.]

Fig.8 and Fig.9 suggest that the condition of Eq.(10) is fulfilled almost in the entire ranges of the number z and limiting radius λ_{rc}. For $[\nu] = 32.5°$ and $\lambda_{rc} = 2.2$, this condition is fulfilled at z

≤ 10. The limiting radius λ_{rc} should take the smallest possible value to reduce the geometric dimensions of the mechanism whilst providing a single-sign curvature path of the driving pin.

Thereby, Figs.5–9 outline the set of the groove cam Geneva mechanisms that provide the double locking of the wheel at its dwell-to-motion and motion-to-dwell transitions, absence of soft impacts in the extreme positions and significantly wider range of the operating time coefficient k_w compared to the conventional Geneva mechanisms. It should be noted that the developed method is not limited by the type of function given by Eq.(20) and can be applied for arbitrary law of motion of the wheel.

5. Synthesis algorithm

The theoretical results obtained in Sections **2–4** can be combined into one algorithm presented in Fig.10. At the first stage, the number z of slots and the operating time coefficient k_w are determined by Eq.(2). At the second stage, the cam profile is checked for the maximum pressure angle ν_{max} due to Eq.(7). As mentioned in Section **4.1**, the symmetry of the cam profile in the zones I and III should be taken into consideration. At the third stage, the cam profile is checked for the minimum curvature radius ρ_{min} due to Eq.(10). Remind that the check is not performed for the zones I and III where the driving pin path is linear. If at least one of the conditions Eq.(7) and Eq.(10) is not fulfilled, the algorithm returns to the first stage.

Repetition of the first three stages leads to the fourth stage which consists in forming the set of pairs z and k_w that satisfy the main and additional conditions of synthesis. The fifth stage is selection of the optimum solution. In general, a smaller value of k_w corresponds to a higher productivity of the machine employing the groove cam Geneva mechanism but also to higher inertial loads on the mechanism. Therefore, a dynamic analysis of the mechanism considering inertial masses attached to the wheel is necessary to evaluate the margin of strength that can be sacrificed in favour of productivity. At the sixth stage, the cam profile is drawn based on the synthesised path of the driving pin.

Since in the present study the centre C of the roller follower 5 is assumed to coincide with the centre A of the driving pin 4 (see Fig.2), i.e. the cam profile is identical to the path of the centre A, the final stage of the algorithm does not require calculations. In the general case, this assumption is not true, and the cam profile is to be drawn based on the path of the driving pin centre A. Obviously, the expressions derived in Sections **3** and **4** become more cumbersome in this case. Nonetheless, the general approach presented in Section **2** and summarised by the algorithm in Fig.10 remains valid.

[insert Figure 10.]

6. Method application

For example, consider a problem of synthesising the Geneva mechanism with operating time coefficient $k_w = 0.3$. Fig.3 shows that none of the number z of slots satisfies $k_w = 0.3$ and $k_{at} = 0$, i.e. the conventional Geneva mechanism cannot provide the required value of k_w. Find the solution using the algorithm proposed in Fig.10, accepting the allowable pressure angle equal to $[\nu] = 41.6°$.

Table 1 presents the pairs z and k_{at} that provide $k_w = 0.3$ due to Eq.(2). The set of solutions is thus $4 \leq z \leq 15$. Fig.5 and Fig.6 show that the condition of Eq.(7) is fulfilled in the zones I–IV for any values of z in the entire range of the limiting radius λ_{rc}, i.e. this condition does not narrow down the set of solutions. On the other hand, due to Fig.7, the condition of Eq.(10) is fulfilled in the zone II at $z \leq 7$. Comparison of Fig.8 and Fig.9 suggests no additional limitations in the zone IV. Thereby, the set of solutions is narrowed down by Eq.(10) to $4 \leq z \leq 7$. Fig.11a presents the synthesised paths of the driving pin for the limit values of z at $\lambda_{rc} = 1$. The solution $z = 4$ provides minimum inertia load on the mechanism, whereas the solution $z = 7$ maximises the machine productivity.

Table 1. Pairs of the number z of slots and additional dwell coefficient k_{at} providing $k_w = 0.3$

z	4	5	6	7	8	9	10	11	12	13	14	15
k_{at}	0.0769	0.231	0.308	0.354	0.385	0.407	0.423	0.436	0.446	0.456	0.462	0.468

Now consider another problem that consists in synthesising the Geneva mechanism with specified number of slots $z = 8$. For the sake of variety, the allowable pressure angle is set equal to $[\nu] = 32.5°$ in this example.

Fig.3 outlines the infinite set of solutions for $z = 8$ in the form of k_{at} ranging between 0 to 0.7. The check of Eq.(7) shows that k_{at} is limited from above by 0.48 in the zones I and III, as shown in Fig.5a, and by 0.46 in the zone II, as shown in Fig.5b. Due to Fig.6 for the zone IV, the limiting radius λ_{rc} may vary between 1 and 2. Further, the check of Eq.(10) shows that k_{at} is limited from above by 0.29 in the zone II, as shown in Fig.7, whilst there are no additional limitations in the zone IV, as shown in Fig.8 and Fig.9. The set of solutions is thereby limited by Eq.(7) and Eq.(10) to the range $0 \le k_{at} \le 0.29$. Fig.11b shows the synthesised paths of the driving pin for the limit values of k_{at} at $\lambda_{rc} = 1$. The solution $k_{at} = 0$ has the same operating time coefficient $k_w = 0.6$ as the conventional Geneva mechanism. In contrast, the solution $k_{at} = 0.29$ corresponds to $k_w = 0.37$, i.e. the groove cam Geneva mechanism synthesised by the algorithm in Fig.10 allows improving the machine productivity by $(1 + 0.6)/(1 + 0.37) \approx 1.17$ times.

[insert Figure 11.]

7. Conclusions

A synthesis method for the groove cam external Geneva mechanisms with increased dwell period is developed which provides the required law of motion of the wheel with account of the conditions limiting the maximum pressure angle ν_{max} and minimum curvature radius ρ_{min} of the cam profile.

It is shown that unlike the conventional Geneva mechanisms, the synthesised groove cam Geneva mechanisms enable:

- arbitrary law of motion of the wheel;
- double locking of the wheel at its dwell-to-motion and motion-to-dwell transitions;
- absence of soft impacts in the extreme positions;
- significantly wider range of the operating time coefficient k_w.

The dimensionless analysis performed for the cycloidal law of motion, number z of slots in range from 3 to 15, additional dwell coefficient k_{at} in range from 0 to 0.7 shows that the operating time coefficient k_w is provided in range from 0.053 to 0.765. The advantages of the synthesised groove cam Geneva mechanisms over the conventional Geneva mechanisms are clearly illustrated by the numerical examples.

Declaration of conflicting interests
The authors declare that there is no conflict of interest.

Funding
The authors received no financial support for the research, authorship, and/or publication of this article.

References

1. Bickford JH. *Mechanisms for intermittent motion*. New York: Industrial Press Inc., 1972, pp.127–138.

2. Chironis NP, Nicholas P. *Mechanisms and mechanical devices sourcebook*. New York: McGraw-Hill, 1991.
3. Prajapati A, Patel C, Pankhania D, et al. Review on Geneva mechanism and its application. *Int J Adv Eng Res Dev* 2017; 4 (2): 425–429.
4. Beltz RK, Hurst JC. Peristaltic pump metering and dispensing system. *Technical Digest - Western Electric Company*, 1975, no.37, pp.3–4.
5. Pazouki ME, Jones JR. The kinematic synthesis of a linkage driven Geneva mechanism. *Mech Mach Theory* 1982; 17 (3): 221–228.
6. Meyer G. A tested method for precise intermittent motion. *Mach Des* 1988; 60 (1): 140–143.
7. Egorov OD, Nadezhdin IV. Use of Geneva mechanisms in industrial robots. *Sov Eng Res* 1988; 8 (11): 134–137.
8. Lee JJ, Cho CC. Improving kinematic and structural performance of Geneva mechanism using the optimal control method. *Proc Inst Mech Eng C J Mech Eng Sci* 2002; 216 (7): 761–774.
9. Kali Sindhur P, Karthik Y, vijay T, et al. Cutting mechanism by giving through Geneva mechanism. *Int J Innov Sci Eng Technol* 2015; 2 (4): 1172–1175.
10. Ujam AJ, Ejeogo G, Onyeneho KC. Development and application of Geneva mechanism for bottle washing. *Am J Eng Res* 2015; 4 (11): 63–73.
11. Zhang E, Wang L. Parametric design and motion analysis of Geneva wheel mechanism based on the UG NX8.5. In: *International Conference on Manufacturing Engineering and Intelligent Materials*, Advances in Engineering, 2017, vol.100, pp.352–356.
12. Sepahpour B. *Kinematic and kinetic analysis of Geneva mechanisms and their applications to synchronization of motion*. PhD Thesis, New Jersey Institute of Technology, 1994.
13. Figliolini G, Rea P, Angeles J. The pure-rolling cam-equivalent of the Geneva mechanism. *Mech Mach Theory* 2006; 41 (11): 1320–1335.
14. Shaohua S, Jifei C. Kinematic analysis on series combined mechanism of elliptic gear and outer Geneva. *Appl Mech Mater* 2013; 312: 42–46.
15. Dijksman EA. Jerk-free Geneva wheel driving. *J Mech* 1966; 1 (3–4): 235–280.
16. Bagci C. Synthesis of double-crank driven mechanisms with adjustable motion and dwell time ratios. *Mech Mach Theory* 1977; 12 (6): 619–638.
17. Yang AT, Hsia LM. Multistage geared Geneva mechanism. *Trans ASME J Mech Des* 1979; 101 (1): 41–46.
18. Fenton RG. Geneva mechanisms connected in series. *Trans ASME J Manuf Sci Eng* 1975; 97: 603–608.
19. Al-Sabeeh AK. Double crank external Geneva mechanism. *Trans ASME J Mech Des* 1993; 115: 666–670.
20. Figliolini G, Rea P. Effects of the design parameters on the synthesis of Geneva mechanisms. *Proc Inst Mech Eng C J Mech Eng Sci* 2012; 227 (9): 2000–2009.
21. Yang AT, Hsia LM. Multistage geared Geneva mechanism. *Trans ASME J Mech Des* 1979; 101: 41–46.
22. Sujan VA, Meggiolaro MA. Dynamic optimization of Geneva mechanisms. In: *International Conference on Gearing, Transmissions and Mechanical Systems*, 2000, pp.687–696.
23. Sadek KSH., Lloyd JL, Smith MR. A new design of Geneva drive to reduce shock loading. *Mech Mach Theory* 1990; 25: 589–595.
24. Cheng CY, Lin Y. Improving dynamic performance of the Geneva mechanism using non-linear spring elements. *Mech Mach Theory* 1995; 30: 119–129.
25. Fenton RG, Zhang Y, Xu J. Development of a new Geneva mechanism with improved kinematic characteristics. *Trans ASME J Mech Des* 1991; 113 (1): 40–45.
26. Lee HP. Design of a Geneva mechanism with curved slots using parametric polynomials. *Mech Mach Theory* 1998; 33 (3): 321–329.
27. Lee JJ, Huang KF. Geometry analysis and optimal design of Geneva mechanisms with curved slots. *Proc Inst Mech Eng C J Mech Eng Sci* 2004; 218 (4): 449–458.

28. Lee JJ, Jan BH. Design of Geneva mechanisms with curved slots for non-undercutting manufacturing. *Mech Mach Theory* 2009; 44 (6): 1192–1200.
29. Li HT. Design of a new kind of curved groove on Geneva mechanism. *J China Agric Univ* 2005; 10: 62–65.
30. DuMont CL, Kurtz AF, Silverstein BD, et al. Design improvement for motion picture film projectors. In: *143rd Technical Conference and Exhibition*, New York, 2001, pp.785–791.
31. Zhang J, Sun S, Tuan HA. Optimization design and analysis of rotary indexing mechanism of tool magazine in machining center. *Jordan J Mech Ind Eng* 2020; 14 (1): 1–6.
32. Heidari M, Atai AA, Shariat Panahi M. An improved Geneva mechanism for optimal kinematic performance. *Proc Inst Mech Eng C J Mech Eng Sci* 2012; 226 (6): 1515–1525.
33. Polyudov OM. *Mechanics of printing machines.* Kyiv: NMKVO, 1991.
34. Uicker JJ, Pennock GR, Shigley JE. *Theory of machines and mechanisms*. 5th ed. New York: Oxford University Press, 2017.

A method to synthesise groove cam Geneva mechanisms with increased dwell period

Viacheslav Pasika[a], Pavlo Nosko[b], Oleksii Nosko[c*], Oleksandr Bashta[b], Volodymyr Heletiy[a], Volodymyr Melnyk[b]

[a] Lviv Polytechnic National University,
Department of Technical Mechanics and Dynamics of Machines, Bandery 32, Lviv, 79013, Ukraine
[b] National Aviation University, Aerospace Faculty, Department of Applied Mechanics and Materials Engineering, Lubomyr Husar 1, Kyiv, 03058, Ukraine
[c] Gdansk University of Technology, Faculty of Mechanical Engineering and Ship Technology, Narutowicza 11/12, Gdansk, 80233, Poland
[*]Corresponding author: oleksii.nosko@pg.edu.pl, https://orcid.org/0000-0002-5259-1426

Abstract
The present study develops a method to synthesise the groove cam Geneva mechanism with increased dwell period. The main condition of the synthesis is to provide the desired law of motion of the wheel. Additional synthesis conditions are the limitation of the maximum pressure angle and the limitation of the minimum curvature radius of the cam profile. Unlike the conventional Geneva mechanisms, the synthesised groove cam Geneva mechanisms enable motion of the wheel due to an arbitrarily specified law, double locking of the wheel at its dwell-to-motion and motion-to-dwell transitions, absence of soft impacts in the extreme positions. The analysis shows that for the cycloidal law of motion, number of slots in range 3 to 15 and additional dwell coefficient in range 0 to 0.7, the operating time coefficient can be provided in wide range from 0.053 to 0.765. The effectiveness of the method is illustrated by numerical examples.

Keywords: Geneva mechanism, groove cam Geneva mechanism, synthesis method, number of wheel slots, operating time coefficient, additional dwell coefficient

Notation

a_{k}	wheel rotation invariant
b_{k}	wheel angular velocity invariant
c_{k}	wheel angular acceleration invariant
k	dimensionless time
k_{at}	additional dwell coefficient
k_{w}	operating time coefficient
l_{AB}	distance between the wheel axis and driving pin axis
l_{OA}	initial crank radius
l_{OB}	distance between the crank rotation axis and wheel axis
r	crank radius
t_{s}	wheel dwell period
t_{t}	wheel motion period
z	number of slots
λ_2	dimensionless distance between the wheel axis and driving pin axis
λ_{a}	dimensionless distance between the crank rotation axis and wheel axis
λ_{r}	dimensionless crank radius
$\lambda_{\mathrm{r1}},...,\lambda_{\mathrm{r4}}$	dimensionless crank radius in the zones I, ..., IV
λ_{rc}	dimensionless limiting radius
ν	pressure angle
$\nu_{\max}$	maximum pressure angle
$[\nu]$	allowable pressure angle
$\rho_{\min}$	dimensionless minimum curvature radius of the cam profile
$[\rho]$	dimensionless allowable curvature radius of the cam profile
φ_1	crank rotation angle
φ_2	wheel rotation angle
$\varphi_{1\Sigma}$	total crank rotation angle
$\varphi_{2\Sigma}$	total wheel rotation angle
ω_1	crank angular velocity
ω_2	wheel angular velocity
$\Delta\varphi$	additional dwell angle

1. Introduction

Increasing speeds and productivity of automatic machines require employment of highly functional and efficient cyclic mechanisms. Geneva mechanisms belong to the cyclic mechanisms commonly used in automatic machines [1–3]. Their application range is extensive and has evolved from mechanical watches and motion-picture projectors to discrete motion drives in robotic manipulators and CNC machines [4–10].

The Geneva mechanisms are simple, technological and undemanding in maintenance. However, like all lever mechanisms, they possess certain disadvantages. First of all, the laws of motion of the wheel are characterised by impact phenomena in its extreme positions, which imposes speed and energy limitations. Moreover, in the Geneva mechanism with a constant crank radius and a fixed number z of slots on the wheel, the operating time coefficient $k_{\mathrm{w}} = {}^{t_{\mathrm{t}}}/_{t_{\mathrm{s}}}$ equal to the ratio of the motion period t_{t} of the wheel to its dwell period t_{s} is governed by the number z as per the equality $k_{\mathrm{w}} = (z-2)/(z+2)$. Adjusting the coefficient k_{w} by changing the number z is not feasible in many practical cases [11].

There is a class of automatic machines and automated lines employing the Geneva mechanism where most technological operations are performed when the wheel is stationary. This class includes but is not limited to engine lathe machines, carousel lathe machines, cutting machines, milling machines, drilling machines, packaging machines, conveyor machines, lining machines. For example, if the Geneva mechanism is used in a bottle filling machine, rotation of the wheel provides placing the consecutive empty bottle under the valve, whilst filling of the bottle with liquid takes place during the dwell period t_{s}. The productivity of such automatic machines can be thus improved by reducing the motion period t_{t} or, in other words, increasing the dwell period t_{s}. However, if large inertial masses are attached to the wheel, the motion period t_{t} cannot be reduced without a significant increase in the wheel angular acceleration and, accordingly, inertial loads.

Further, the disadvantages of the Geneva mechanisms include the fact that the wheel is locked solely by a locking ring [12]. As the driving pin of the crank enters the slot, the edge of the locking ring, which is rigidly connected to the crank, comes out of contact with the wheel. High accuracy should be, therefore, guaranteed for the mutual location between the crank and locking ring. Errors in the manufacture and installation of the mechanism and its wear lead to the occurrence of unwanted gaps. This, in its turn, results in non-simultaneous entry of the driving pin into the slot and exit of the locking ring from contact, which is accompanied by increased impact loads. A similar situation is observed when the driving pin leaves the slot.

Several approaches have been proposed to improve the dynamic performance of the Geneva mechanisms. The first approach implies application of compound mechanisms to eliminate soft impacts (discontinuous accelerations) in the extreme positions [13–22]. Two or more mechanisms are connected in series so that the angular acceleration of the wheel changes continuously during its motion. This approach inevitably introduces extra components to the system. The second approach is using damping elements in the Geneva mechanism in order to reduce the impact loads [23, 24], which also leads to extra components in the system. The third approach is to modify the geometry of the slots [25–29]. Curvilinear slots are designed to provide the desired law of motion, similarly as in cam mechanisms. Although processing of the curvilinear slots is resource consuming, the approach enables adjusting the dwell period t_{s} even for a fixed number z of slots.

The study [30] investigates the applicability of the wheel with barrel-shaped slots, called ‘Quickermittent’, for motion picture film projectors. Such a mechanism allows to reduce the indexing time whilst maintaining control over the loads on the film and mechanism itself. However, due to the fact that the slot is wider in its middle part, the driving pin can hit the walls of the slot, which affects adversely on the motion stability, especially at low rotational speeds. In addition, Quickermittent mechanisms tend to be noisier than the Geneva mechanisms.

A double-pins without locking arc Geneva mechanism is developed in the study [31]. The proposed mechanism has two driving pins in contrast to the conventional Geneva mechanism with one driving pin, resulting in two times higher angular velocity of the wheel. Smaller impact loads in

the mechanism are achieved by optimising the transitional part of the slot, which implies, however, higher manufacturing costs.

The studies [2, 8, 32, 33] suggest that the functionality of the Geneva mechanism can be substantially extended by introducing a groove cam element. The groove cam Geneva mechanism comprises input crank 1, output wheel 2, groove cam 3, driving pin 4 and roller follower 5, as shown in Fig.1. The crank 1 rotates at constant angular velocity ω_1 and simultaneously moves radially due to the path of the roller follower 5 along the groove of the cam 3. The driving pin 4 on the crank 1 brings the wheel 2 in motion. Thus, the mechanism makes use of the cam 3 to control the radius of action of the driving pin 4, which provides the necessary kinematic characteristics of the wheel 2.

[insert Figure 1.]

The analysis of the above-mentioned studies indicates a lack of research devoted to solving the problem of synthesising the groove cam Geneva mechanism and analysing the influence of different parameters on its performance. The purpose of the present study is to develop a method to synthesise the groove cam Geneva mechanism with increased dwell period that satisfies the desired law of motion of the wheel (main condition), allowable pressure angle and allowable curvature radius of the cam profile (additional conditions). The following tasks are solved to achieve this purpose: development of the general approach to determining the path of the driving pin due to the specified operating time coefficient k_{w} (Section 2); formulation of the additional conditions of synthesis (Section 3); development of the method to synthesise the driving pin path (Section 4); development of the synthesis algorithm (Section 5); illustration of the method application (Section 6).

2. General approach to determining the driving pin path

A detailed schematic of the groove cam Geneva mechanism is shown in Fig.2. The numbering of the elements in the schematic corresponds to Fig.1. In addition to the input crank 1, output wheel 2, groove cam 3, driving pin 4 and roller follower 5, Fig.2 presents the locking ring 6. To reduce the number of parameters in the present study and simplify analysis, the roller follower 5 is assumed to have a common axis with the driving pin 4, i.e. the centre C of the roller follower 5 coincides with the centre A of the driving pin 4. Under this assumption, the profile of the cam 3 coincides with the path of the centre A of the driving pin 4.

[insert Figure 2.]

Imagine that the driving pin 4 enters the slot of the wheel 2 at the moment when the crank 1 and slot are mutually perpendicular. The driving pin 4 passes then along the slot from the position A to the position A_1, which corresponds to a certain rotation angle $\Delta\varphi$ of the crank 1. In this interval, the wheel 2 is stationary due to its locking by the ring 6 and motion of the driving pin 4 along the line AA_1. As the crank 1 rotates by the angle $\Delta\varphi$, the wheel 2 is brought in motion. Apparently, the described situation corresponds to an increase in the dwell period t_{s} of the wheel 2. The angle $\Delta\varphi$ is referred to as 'additional dwell angle'.

There is thus a principal difference between the operation of the conventional Geneva mechanism and that of the groove cam Geneva mechanism. In the former, the locking of the wheel at its dwell-to-motion and motion-to-dwell transitions is performed solely by the locking ring, whereas in the latter it is performed by both locking ring 6 and driving pin 4.

Derive an analytical expression for the operating time coefficient k_{w}. Introduce the total crank rotation angle $\varphi_{1\Sigma}$ and total wheel rotation angle $\varphi_{2\Sigma}$ as

$$\varphi_{1\Sigma} = \pi\left(1 - \frac{2}{z}\right);$$

$$\varphi_{2\Sigma} = \frac{2\pi}{z}$$

Further, express the motion period t_t and dwell period t_s in the form

$$t_t = \frac{\varphi_{1\Sigma} - 2\Delta\varphi}{\omega_1};$$

$$t_s = \frac{2\pi - \varphi_{1\Sigma} + 2\Delta\varphi}{\omega_1}$$

Based on the equations above, the operating time coefficient k_w can be expressed as follows:

$$k_w = \frac{t_t}{t_s} = \frac{\pi(z-2)/z - 2\Delta\varphi}{\pi(z+2)/z + 2\Delta\varphi} \quad (1)$$

After defining the additional dwell coefficient as the ratio

$$k_{at} = \frac{2\Delta\varphi}{\varphi_{1\Sigma}}$$

Eq.(1) can be rewritten in the following manner:

$$k_w = \frac{(z-2)(1-k_{at})}{2z - (z-2)(1-k_{at})} \quad (2)$$

Apparently, the operating time coefficient k_w is reduced at $\Delta\varphi > 0$ and, accordingly, $k_{at} > 0$. As the coefficient k_{at} tends to 1, the additional dwell angle $\Delta\varphi$ increases significantly along with the geometric dimensions of the mechanism (see Fig.2). It is reasonable, therefore, to limit k_{at}, and the present study accepts that $k_{at} \leq 0.7$. Due to the fact that the number z of slots cannot be less than 3, whilst the Geneva mechanisms with $z > 15$ are rarely met in practice, the number z is accepted to be in range from 3 to 15.

Fig.3 illustrates the dependence of the operating time coefficient k_w on the additional dwell coefficient k_{at} and number z due to Eq.(2). The analysis shows that for the conventional Geneva mechanism ($k_{at} = 0$), the coefficient k_w changes from 0.2 to 0.765. By contrast, the groove cam Geneva mechanism has a significantly wider range of the coefficient k_w from 0.053 to 0.765 at $0 < k_{at} \leq 0.7$. Note that the coefficient k_w is more sensitive to the variation of k_{at} at smaller values of k_{at}.

[insert Figure 3.]

Considering Fig.2, introduce the dimensionless crank radius λ_r, dimensionless distance λ_2 between the driving pin axis A and wheel axis B, dimensionless distance λ_a between the crank rotation axis O and wheel axis B as

$$\lambda_r = \frac{r}{l_{OA}};$$

$$\lambda_2 = \frac{l_{AB}}{l_{OA}};$$

$$\lambda_a = \frac{l_{OB}}{l_{OA}} = \frac{1}{\sin(\pi/z)}$$

where r is the crank radius, i.e. the distance between the crank rotation axis O and driving pin axis A; l_{AB} is the distance between the driving pin axis A and wheel axis B; l_{OB} is the distance between the crank rotation axis O and wheel axis B; l_{OA} is the initial crank radius for the perpendicular position between the crank and slot.

Writing the equation of closed vector circuit in the form

$$\bar{\lambda}_{\mathrm{r}} + \bar{\lambda}_2 = \bar{\lambda}_{\mathrm{a}}$$

and projecting it on the horizontal and vertical axes yield that

$$\lambda_{\mathrm{r}} = \lambda_{\mathrm{a}} \frac{\sin\left(\pi/z - \varphi_2\right)}{\cos\left(\varphi_1 + \varphi_2\right)};$$

$$\lambda_2 = \lambda_{\mathrm{a}} \frac{\cos\left(\pi/z + \varphi_1\right)}{\cos\left(\varphi_1 + \varphi_2\right)} \tag{3}$$

where φ_1 and φ_2 are the rotation angles of the respective crank and wheel.

Further, represent the rotation angles of the respective crank and wheel in the form

$$\varphi_1 = k\varphi_{1\Sigma};$$

$$\varphi_2 = a_{\mathrm{k}}\varphi_{2\Sigma}$$

where $k = \varphi_1/\varphi_{1\Sigma}$ is the dimensionless time; a_{k} is the wheel rotation invariant. Then the derivatives of the radius λ_{r} with respect to φ_1 read

$$\lambda'_{\mathrm{r}} = \frac{d\lambda_{\mathrm{r}}}{d\varphi_1} = \frac{\lambda_{\mathrm{a}}}{\cos^2\left(\varphi_1 + \varphi_2\right)}\left(\sin\left(\varphi_1 + \varphi_2\right)\sin\left(\frac{\pi}{z} - \varphi_2\right) - \varphi'_2\cos\left(\frac{\pi}{z} + \varphi_1\right)\right);$$

$$\lambda''_{\mathrm{r}} = \frac{d^2\lambda_{\mathrm{r}}}{d\varphi_1^2} = -\frac{\lambda_{\mathrm{a}}}{\cos^3\left(\varphi_1 + \varphi_2\right)}\left(\varphi''_2\cos\left(\varphi_1 + \varphi_2\right)\cos\left(\frac{\pi}{z} + \varphi_1\right) + 2\varphi'_2\right.$$
$$\left(\left(1 + \varphi'_2\right)\cos\left(\varphi_1 + \varphi_2\right)\sin\left(\frac{\pi}{z} + \varphi_1\right) - \left(2 + \varphi'_2\right)\sin\left(\frac{\pi}{z} - \varphi_2\right)\right)$$
$$\left. + \left(1 + \sin^2\left(\varphi_1 + \varphi_2\right)\right)\sin\left(\frac{\pi}{z} - \varphi_2\right)\right) \tag{4}$$

with

$$\varphi'_2 = \frac{d\varphi_2}{d\varphi_1} = b_{\mathrm{k}}\frac{\varphi_{2\Sigma}}{\varphi_{1\Sigma}};$$

$$\varphi''_2 = \frac{d^2\varphi_2}{d\varphi_1^2} = c_{\mathrm{k}}\frac{\varphi_{2\Sigma}}{\varphi_{1\Sigma}^2} \tag{5}$$

where $b_{\mathrm{k}} = da_{\mathrm{k}}/dk$ and $c_{\mathrm{k}} = db_{\mathrm{k}}/dk$ are the wheel angular velocity and acceleration invariants.

Thus, as the crank radius λ_{r} changes due to Eq.(3), the wheel moves according to the prescribed law with rotation invariant a_{k}. Remember that the expressions for λ_{r}, λ'_{r}, λ''_{r} given by Eqs.(3)–(5) are valid if the wheel motion starts from the perpendicular position between the crank and slot.

3. Additional conditions of synthesis

Since the studied mechanism (see Fig.2) includes a cam mechanism in the form of the roller follower in contact with the groove cam, the additional conditions of synthesis arise, as considered next.

3.1. Limitation condition for the maximum pressure angle

In order to prevent jamming in the cam mechanism, the maximum value $\nu_{\max}$ of the pressure angle

$$\nu = \arctan\frac{\lambda_{\mathrm{r}}'}{\lambda_{\mathrm{r}}} \tag{6}$$

should not exceed the allowable pressure angle $[\nu]$. The corresponding condition limiting the maximum pressure angle $\nu_{\max}$ is formulated as

$$\nu_{\max} \leq [\nu] \tag{7}$$

The allowable pressure angle $[\nu]$ is chosen depending on the angular velocity and load in the cam mechanism. In most engineering applications, the value of $[\nu]$ is in range from 30° to 45°. In the present study, $[\nu]$ is accepted to be between 32.5° and 41.6°, which corresponds to the case of rotary tables like Vertex Precision Tilting Rotary Table VUT used in carousel lathe machines, cutting machines, milling machines, drilling machines and conveyor machines [33].

3.2. Limitation condition for the minimum curvature radius of the cam profile

In order to prevent sharpening and interference of the cam profile, it is necessary to limit from below its minimum curvature radius $\rho_{\min}$. The allowable curvature radius $[\rho]$ of the cam profile is determined by the dimensionless expression [34]

$$[\rho] = \max\left\{\frac{\lambda_{\mathrm{r}}'}{\tan[\nu]} - \lambda_{\mathrm{r}} + \min\lambda_{\mathrm{r}}\right\} \tag{8}$$

The minimum curvature radius $\rho_{\min}$ of the cam profile is derived from the known formula for the radius of curvature given in polar coordinates as

$$\rho_{\min} = \min\left\{\frac{\left(\lambda_{\mathrm{r}}^2 + \left(\lambda_{\mathrm{r}}'\right)^2\right)^{3/2}}{\lambda_{\mathrm{r}}^2 + 2\left(\lambda_{\mathrm{r}}'\right)^2 - \lambda_{\mathrm{r}}\lambda_{\mathrm{r}}''}\right\} \tag{9}$$

The condition limiting the minimum curvature radius $\rho_{\min}$ takes then the following form:

$$\rho_{\min} \geq [\rho] \tag{10}$$

Thus, the additional conditions of synthesis include Eq.(7) limiting the maximum pressure angle $\nu_{\max}$ and Eq.(10) limiting the minimum curvature radius $\rho_{\min}$ of the cam profile.

4. Method to synthesise the driving pin path

Fig.4 shows the characteristic zones of the crank motion: I — linear path of the driving pin, stationary wheel; II — path of the driving pin for the wheel motion period; III — linear path of the driving pin, stationary wheel; IV — path of the driving pin which provides a smooth conjugation of the end of the zone III and the start of the zone I. The crank radius λ_{r} is determined next for each zone.

[insert Figure 4.]

Zone I starts in the position *A* when the driving pin enters the slot, and it ends in the position A_1 when the crank rotates by the additional dwell angle $\Delta\varphi$. The rotation angle φ_1 of the crank

changes, thereby, from 0 to $\Delta\varphi$. Considering the fact that the wheel is stationary, i.e. $\varphi_2 = 0$, a simplified expression for the crank radius λ_{r1} is derived in the form

$$\lambda_{r1} = \frac{1}{\cos\varphi_1} \tag{11}$$

Zone II starts in the position A_1 and ends in the position A_1'. The wheel moves according to the prescribed law. The crank rotation angle φ_1 changes from $\Delta\varphi$ to $(\varphi_{1\Sigma} - \Delta\varphi)$. The crank radius λ_{r2} is found from Eqs.(3)–(5).

Zone III starts in the position A_1' and ends in the position A'. The motion of the driving pin occurs similarly to that in the zone I. The crank rotation angle φ_1 changes from $(\varphi_{1\Sigma} - \Delta\varphi)$ to $\varphi_{1\Sigma}$. Since $\varphi_2 = \varphi_{2\Sigma} = 2\pi/z$, the expression for the crank radius λ_{r3} reads

$$\lambda_{r3} = -\frac{1}{\cos\left(2\pi/z + \varphi_1\right)}$$

Zone IV starts in the position A' and ends in the position A. Accordingly, the crank rotation angle φ_1 changes from $\varphi_{1\Sigma}$ to 2π. The crank radius λ_{r4} can be defined in the form of polynomial

$$\lambda_{r4} = \sum_{i=1}^{n} a_i \varphi_1^{i-1} \tag{12}$$

where n is the number of the conditions imposed on the crank radius λ_{r4}.

The boundary conditions are formulated to prevent soft impacts at the start of the zone I in the position A and at the end of the zone III in the position A'. This can be achieved by smooth conjugation of the crank radius and its first three derivatives, i.e.

$$\begin{aligned}
\lambda_{r4} &= \lambda_{r3}\big|_{\varphi_1 = \varphi_{1\Sigma}};\\
\lambda_{r4}' &= \lambda_{r3}'\big|_{\varphi_1 = \varphi_{1\Sigma}};\\
\lambda_{r4}'' &= \lambda_{r3}''\big|_{\varphi_1 = \varphi_{1\Sigma}};\\
\lambda_{r4}''' &= \lambda_{r3}'''\big|_{\varphi_1 = \varphi_{1\Sigma}}
\end{aligned} \tag{13}$$

and

$$\begin{aligned}
\lambda_{r4}\big|_{\varphi_1 = 2\pi} &= \lambda_{r1}\big|_{\varphi_1 = 0};\\
\lambda_{r4}'\big|_{\varphi_1 = 2\pi} &= \lambda_{r1}'\big|_{\varphi_1 = 0};\\
\lambda_{r4}''\big|_{\varphi_1 = 2\pi} &= \lambda_{r1}''\big|_{\varphi_1 = 0};\\
\lambda_{r4}'''\big|_{\varphi_1 = 2\pi} &= \lambda_{r1}'''\big|_{\varphi_1 = 0}
\end{aligned} \tag{14}$$

Since there is infinite number of functions satisfying Eq.(13) and Eq.(14), additional conditions should be formulated. In the bisector of the zone IV, which corresponds to the crank rotation angle $\varphi_1 = \varphi_c = \varphi_{1\Sigma}/2 + \pi$, the crank radius λ_{r4} is set equal to the dimensionless limiting radius λ_{rc}, i.e.

$$\lambda_{r4}\big|_{\varphi_1 = \varphi_c} = \lambda_{rc} \tag{15}$$

and the rate of change of λ_{r4} is set equal to zero, i.e.

$$\lambda_{r4}'\big|_{\varphi_1 = \varphi_c} = 0 \tag{16}$$

Thereby, the total number of the conditions given by Eqs.(13)–(16) equals $n = 10$. These conditions lead to the following system of equations with respect to the coefficients a_i in Eq.(12):

$$\begin{pmatrix} 1 & \varphi_{1\Sigma} & \varphi_{1\Sigma}^2 & \varphi_{1\Sigma}^3 & \varphi_{1\Sigma}^4 & \varphi_{1\Sigma}^5 & \varphi_{1\Sigma}^6 & \varphi_{1\Sigma}^7 & \varphi_{1\Sigma}^8 & \varphi_{1\Sigma}^9 \\ 0 & 1 & 2\varphi_{1\Sigma} & 3\varphi_{1\Sigma}^2 & 4\varphi_{1\Sigma}^3 & 5\varphi_{1\Sigma}^4 & 6\varphi_{1\Sigma}^5 & 7\varphi_{1\Sigma}^6 & 8\varphi_{1\Sigma}^7 & 9\varphi_{1\Sigma}^8 \\ 0 & 0 & 2 & 6\varphi_{1\Sigma} & 12\varphi_{1\Sigma}^2 & 20\varphi_{1\Sigma}^3 & 30\varphi_{1\Sigma}^4 & 42\varphi_{1\Sigma}^5 & 56\varphi_{1\Sigma}^6 & 72\varphi_{1\Sigma}^7 \\ 0 & 0 & 0 & 6 & 24\varphi_{1\Sigma} & 60\varphi_{1\Sigma}^2 & 120\varphi_{1\Sigma}^3 & 210\varphi_{1\Sigma}^4 & 336\varphi_{1\Sigma}^5 & 504\varphi_{1\Sigma}^6 \\ 1 & \varphi_{\mathrm{e}} & \varphi_{\mathrm{e}}^2 & \varphi_{\mathrm{e}}^3 & \varphi_{\mathrm{e}}^4 & \varphi_{\mathrm{e}}^5 & \varphi_{\mathrm{e}}^6 & \varphi_{\mathrm{e}}^7 & \varphi_{\mathrm{e}}^8 & \varphi_{\mathrm{e}}^9 \\ 0 & 1 & 2\varphi_{\mathrm{e}} & 3\varphi_{\mathrm{e}}^2 & 4\varphi_{\mathrm{e}}^3 & 5\varphi_{\mathrm{e}}^4 & 6\varphi_{\mathrm{e}}^5 & 7\varphi_{\mathrm{e}}^6 & 8\varphi_{\mathrm{e}}^7 & 9\varphi_{\mathrm{e}}^8 \\ 0 & 0 & 2 & 6\varphi_{\mathrm{e}} & 12\varphi_{\mathrm{e}}^2 & 20\varphi_{\mathrm{e}}^3 & 30\varphi_{\mathrm{e}}^4 & 42\varphi_{\mathrm{e}}^5 & 56\varphi_{\mathrm{e}}^6 & 72\varphi_{\mathrm{e}}^7 \\ 0 & 0 & 0 & 6 & 24\varphi_{\mathrm{e}} & 60\varphi_{\mathrm{e}}^2 & 120\varphi_{\mathrm{e}}^3 & 210\varphi_{\mathrm{e}}^4 & 336\varphi_{\mathrm{e}}^5 & 504\varphi_{\mathrm{e}}^6 \\ 1 & \varphi_{\mathrm{c}} & \varphi_{\mathrm{c}}^2 & \varphi_{\mathrm{c}}^3 & \varphi_{\mathrm{c}}^4 & \varphi_{\mathrm{c}}^5 & \varphi_{\mathrm{c}}^6 & \varphi_{\mathrm{c}}^7 & \varphi_{\mathrm{c}}^8 & \varphi_{\mathrm{c}}^9 \\ 0 & 1 & 2\varphi_{\mathrm{c}} & 3\varphi_{\mathrm{c}}^2 & 4\varphi_{\mathrm{c}}^3 & 5\varphi_{\mathrm{c}}^4 & 6\varphi_{\mathrm{c}}^5 & 7\varphi_{\mathrm{c}}^6 & 8\varphi_{\mathrm{c}}^7 & 9\varphi_{\mathrm{c}}^8 \end{pmatrix} \begin{pmatrix} a_1 \\ a_2 \\ a_3 \\ a_4 \\ a_5 \\ a_6 \\ a_7 \\ a_8 \\ a_9 \\ a_{10} \end{pmatrix} = \begin{pmatrix} \lambda_{\mathrm{r}3}\big|_{\varphi_{1\Sigma}} \\ \lambda'_{\mathrm{r}3}\big|_{\varphi_{1\Sigma}} \\ \lambda''_{\mathrm{r}3}\big|_{\varphi_{1\Sigma}} \\ \lambda'''_{\mathrm{r}3}\big|_{\varphi_{1\Sigma}} \\ \lambda_{\mathrm{r}1}\big|_0 \\ \lambda'_{\mathrm{r}1}\big|_0 \\ \lambda''_{\mathrm{r}1}\big|_0 \\ \lambda'''_{\mathrm{r}1}\big|_0 \\ \lambda_{\mathrm{rc}} \\ 0 \end{pmatrix} \tag{17}$$

where φ_{e} stands for 2π for shorter notation.

Now it is turn to determine the maximum pressure angle $\nu_{\max}$ and minimum curvature radius $\rho_{\min}$ of the cam profile for each zone and compare them to the allowable values $[\nu]$ and $[\rho]$, respectively.

4.1. Limitation condition for the maximum pressure angle

Zone I. Substitution of Eq.(11) into Eq.(6) results in the pressure angle $\nu = \varphi_1$. Since the crank rotation angle φ_1 changes from 0 to $\Delta\varphi$, it is true that the maximum pressure angle equals $\nu_{\max} = \Delta\varphi$. The condition of Eq.(7) is thus fulfilled if $\Delta\varphi \le [\nu]$ or, taking account of Eq.(1) and Eq.(2), if

$$k_{\mathrm{at}} \le \frac{2z}{\pi(z-2)}[\nu] \tag{18}$$

Fig.5a shows the range of the additional dwell coefficient k_{at} that satisfies Eq.(18). The coefficient k_{at} can take any value between 0 and 0.7 for $z \in \{3,4\}$. As the number z of slots increases, the upper limit of the range decreases. For $z = 15$, it equals 0.417 at $[\nu] = 32.5°$ and 0.532 at $[\nu] = 41.6°$

[insert Figure 5.]

Zone II. Substitution of Eq.(3) and Eq.(4) into Eq.(6) allows deriving the expression of the pressure angle ν in the form

$$\tan\nu = \frac{\sin(\varphi_1+\varphi_2)\sin(\pi/z-\varphi_2) - \varphi_2'\cos(\pi/z+\varphi_1)}{\cos(\varphi_1+\varphi_2)\sin(\pi/z-\varphi_2)} \tag{19}$$

Assume that the wheel moves according to the cycloidal law

$$a_{\mathrm{k}} = k - \frac{\sin(2\pi k)}{2\pi} \tag{20}$$

which is widespread in the cyclic mechanisms, providing zero angular acceleration of the wheel in its extreme positions, i.e. at the start and end of its motion period.

The maximum pressure angle $\nu_{\max}$ is determined based on Eq.(19) and Eq.(20). Fig.5b shows the corresponding range of the coefficient k_{at} satisfying Eq.(7). As in the case of zone I, the coefficient k_{at} can be arbitrary from 0 to 0.7 for $z \in \{3,4\}$. As the number z increases, the upper

limit of the range decreases. For $z = 15$, it equals 0.375 at $[\nu] = 32.5°$ and 0.506 at $[\nu] = 41.6°$. Comparison of Fig.5a and Fig.5b shows that the coefficient k_{at} is smaller in the zone II for any z.

Zone III. Since the zones I and III are symmetrical about the vertical axis (see Fig.4), similar conclusions can be drawn here as for the zone I.

Zone IV. The crank radius λ_{r4} represents the polynomial of Eq.(12) with the coefficients a_i satisfying Eq.(17). The dependence of the maximum pressure angle ν_{max} on the number z and limiting radius λ_{rc} is obtained based on Eq.(6). Fig.6 shows the relevant data for the limiting radius λ_{rc} that changes from 1 to 2.2 with step 0.2. It is seen that for $[\nu] = 32.5°$, the condition of Eq.(7) is fulfilled at $1 \le \lambda_{rc} \le 2$ and any z, as well as at $\lambda_{rc} = 2.2$ and $z \le 7$. For $[\nu] = 41.6°$, the entire range of λ_{rc} satisfies the condition of Eq.(7). Note that the maximum pressure angle ν_{max} increases with increasing λ_{rc}.

[insert Figure 6.]

Summarising the results for all zones leads to the conclusion that the condition of Eq.(7) limiting the maximum pressure angle ν_{max} can be fulfilled for any z. As the number z increases, the upper limit of the coefficient k_{at} decreases. For $[\nu] = 32.5°$, it equals 0.7 at $z = 3$ and 0.375 at $z = 15$, whilst for $[\nu] = 41.6°$, it is about 1.3 times larger. The coefficient k_{at} should be chosen according to the results obtained for the zone II (see Fig.5b). Additionally, the limiting radius λ_{rc} should be specified as small as possible to reduce the maximum pressure angle ν_{max}.

4.2. Limitation condition of the minimum curvature radius of the cam profile

Zone I. Since the path AA_1 of the driving pin is linear (see Fig.4), the curvature radius of the cam profile is infinitely large.

Zone II. Substitution of Eq.(20) into Eqs.(3)–(5) allows determining the allowable curvature radius $[\rho]$ of the cam profile due to Eq.(8) and the minimum curvature radius ρ_{min} of the cam profile due to Eq.(9). Fig.7 shows the range of the coefficient k_{at} satisfying the condition of Eq.(10) in dependence on the number z. The analysis reveals that for $[\nu] = 32.5°$, the synthesis of the driving pin path is possible at $z \ge 4$. The coefficient k_{at} is in range from 0 to 0.29 at $4 \le z \le 13$ and in range from 0 to 0.28 at $z \in \{14,15\}$. As for $[\nu] = 41.6°$, the condition of Eq.(10) is fulfilled for any z. The upper limit of the coefficient k_{at} equals 0.34 at $z = 3$, 0.37 at $z \in \{4,5,6,13,14,15\}$ and 0.38 at $7 \le z \le 12$.

[insert Figure 7.]

Zone III. Similar conclusions are valid as for the zone I due to the symmetry of the zones I and III about the vertical axis (see Fig.4).

Zone IV. The crank radius λ_{r4} is described by the polynomial Eq.(12) with the coefficients a_i satisfying Eq.(17). Fig.8 shows the allowable curvature radius $[\rho]$ of the cam profile determined based on Eq.(8). Fig.9 shows the minimum curvature radius ρ_{min} of the cam profile determined by Eq.(9).

[insert Figure 8.]

[insert Figure 9.]

Fig.8 and Fig.9 suggest that the condition of Eq.(10) is fulfilled almost in the entire ranges of the number z and limiting radius λ_{rc}. For $[\nu] = 32.5°$ and $\lambda_{rc} = 2.2$, this condition is fulfilled at z

≤ 10. The limiting radius λ_{rc} should take the smallest possible value to reduce the geometric dimensions of the mechanism whilst providing a single-sign curvature path of the driving pin.

Thereby, Figs.5–9 outline the set of the groove cam Geneva mechanisms that provide the double locking of the wheel at its dwell-to-motion and motion-to-dwell transitions, absence of soft impacts in the extreme positions and significantly wider range of the operating time coefficient k_w compared to the conventional Geneva mechanisms. It should be noted that the developed method is not limited by the type of function given by Eq.(20) and can be applied for arbitrary law of motion of the wheel.

5. Synthesis algorithm

The theoretical results obtained in Sections **2–4** can be combined into one algorithm presented in Fig.10. At the first stage, the number z of slots and the operating time coefficient k_w are determined by Eq.(2). At the second stage, the cam profile is checked for the maximum pressure angle ν_{max} due to Eq.(7). As mentioned in Section **4.1**, the symmetry of the cam profile in the zones I and III should be taken into consideration. At the third stage, the cam profile is checked for the minimum curvature radius ρ_{min} due to Eq.(10). Remind that the check is not performed for the zones I and III where the driving pin path is linear. If at least one of the conditions Eq.(7) and Eq.(10) is not fulfilled, the algorithm returns to the first stage.

Repetition of the first three stages leads to the fourth stage which consists in forming the set of pairs z and k_w that satisfy the main and additional conditions of synthesis. The fifth stage is selection of the optimum solution. In general, a smaller value of k_w corresponds to a higher productivity of the machine employing the groove cam Geneva mechanism but also to higher inertial loads on the mechanism. Therefore, a dynamic analysis of the mechanism considering inertial masses attached to the wheel is necessary to evaluate the margin of strength that can be sacrificed in favour of productivity. At the sixth stage, the cam profile is drawn based on the synthesised path of the driving pin.

Since in the present study the centre C of the roller follower 5 is assumed to coincide with the centre A of the driving pin 4 (see Fig.2), i.e. the cam profile is identical to the path of the centre A, the final stage of the algorithm does not require calculations. In the general case, this assumption is not true, and the cam profile is to be drawn based on the path of the driving pin centre A. Obviously, the expressions derived in Sections **3** and **4** become more cumbersome in this case. Nonetheless, the general approach presented in Section **2** and summarised by the algorithm in Fig.10 remains valid.

[insert Figure 10.]

6. Method application

For example, consider a problem of synthesising the Geneva mechanism with operating time coefficient $k_w = 0.3$. Fig.3 shows that none of the number z of slots satisfies $k_w = 0.3$ and $k_{at} = 0$, i.e. the conventional Geneva mechanism cannot provide the required value of k_w. Find the solution using the algorithm proposed in Fig.10, accepting the allowable pressure angle equal to $[\nu] = 41.6°$.

Table 1 presents the pairs z and k_{at} that provide $k_w = 0.3$ due to Eq.(2). The set of solutions is thus $4 \leq z \leq 15$. Fig.5 and Fig.6 show that the condition of Eq.(7) is fulfilled in the zones I–IV for any values of z in the entire range of the limiting radius λ_{rc}, i.e. this condition does not narrow down the set of solutions. On the other hand, due to Fig.7, the condition of Eq.(10) is fulfilled in the zone II at $z \leq 7$. Comparison of Fig.8 and Fig.9 suggests no additional limitations in the zone IV. Thereby, the set of solutions is narrowed down by Eq.(10) to $4 \leq z \leq 7$. Fig.11a presents the synthesised paths of the driving pin for the limit values of z at $\lambda_{rc} = 1$. The solution $z = 4$ provides minimum inertia load on the mechanism, whereas the solution $z = 7$ maximises the machine productivity.

Table 1. Pairs of the number z of slots and additional dwell coefficient k_{at} providing $k_w = 0.3$

z	4	5	6	7	8	9	10	11	12	13	14	15
k_{at}	0.0769	0.231	0.308	0.354	0.385	0.407	0.423	0.436	0.446	0.456	0.462	0.468

Now consider another problem that consists in synthesising the Geneva mechanism with specified number of slots $z = 8$. For the sake of variety, the allowable pressure angle is set equal to $[\nu] = 32.5°$ in this example.

Fig.3 outlines the infinite set of solutions for $z = 8$ in the form of k_{at} ranging between 0 to 0.7. The check of Eq.(7) shows that k_{at} is limited from above by 0.48 in the zones I and III, as shown in Fig.5a, and by 0.46 in the zone II, as shown in Fig.5b. Due to Fig.6 for the zone IV, the limiting radius λ_{rc} may vary between 1 and 2. Further, the check of Eq.(10) shows that k_{at} is limited from above by 0.29 in the zone II, as shown in Fig.7, whilst there are no additional limitations in the zone IV, as shown in Fig.8 and Fig.9. The set of solutions is thereby limited by Eq.(7) and Eq.(10) to the range $0 \le k_{at} \le 0.29$. Fig.11b shows the synthesised paths of the driving pin for the limit values of k_{at} at $\lambda_{rc} = 1$. The solution $k_{at} = 0$ has the same operating time coefficient $k_w = 0.6$ as the conventional Geneva mechanism. In contrast, the solution $k_{at} = 0.29$ corresponds to $k_w = 0.37$, i.e. the groove cam Geneva mechanism synthesised by the algorithm in Fig.10 allows improving the machine productivity by $(1 + 0.6)/(1 + 0.37) \approx 1.17$ times.

[insert Figure 11.]

7. Conclusions

A synthesis method for the groove cam external Geneva mechanisms with increased dwell period is developed which provides the required law of motion of the wheel with account of the conditions limiting the maximum pressure angle ν_{max} and minimum curvature radius ρ_{min} of the cam profile.

It is shown that unlike the conventional Geneva mechanisms, the synthesised groove cam Geneva mechanisms enable:

- arbitrary law of motion of the wheel;
- double locking of the wheel at its dwell-to-motion and motion-to-dwell transitions;
- absence of soft impacts in the extreme positions;
- significantly wider range of the operating time coefficient k_w.

The dimensionless analysis performed for the cycloidal law of motion, number z of slots in range from 3 to 15, additional dwell coefficient k_{at} in range from 0 to 0.7 shows that the operating time coefficient k_w is provided in range from 0.053 to 0.765. The advantages of the synthesised groove cam Geneva mechanisms over the conventional Geneva mechanisms are clearly illustrated by the numerical examples.

Declaration of conflicting interests
The authors declare that there is no conflict of interest.

Funding
The authors received no financial support for the research, authorship, and/or publication of this article.

References

1. Bickford JH. *Mechanisms for intermittent motion*. New York: Industrial Press Inc., 1972, pp.127–138.

2. Chironis NP, Nicholas P. *Mechanisms and mechanical devices sourcebook*. New York: McGraw-Hill, 1991.
3. Prajapati A, Patel C, Pankhania D, et al. Review on Geneva mechanism and its application. *Int J Adv Eng Res Dev* 2017; 4 (2): 425–429.
4. Beltz RK, Hurst JC. Peristaltic pump metering and dispensing system. *Technical Digest - Western Electric Company*, 1975, no.37, pp.3–4.
5. Pazouki ME, Jones JR. The kinematic synthesis of a linkage driven Geneva mechanism. *Mech Mach Theory* 1982; 17 (3): 221–228.
6. Meyer G. A tested method for precise intermittent motion. *Mach Des* 1988; 60 (1): 140–143.
7. Egorov OD, Nadezhdin IV. Use of Geneva mechanisms in industrial robots. *Sov Eng Res* 1988; 8 (11): 134–137.
8. Lee JJ, Cho CC. Improving kinematic and structural performance of Geneva mechanism using the optimal control method. *Proc Inst Mech Eng C J Mech Eng Sci* 2002; 216 (7): 761–774.
9. Kali Sindhur P, Karthik Y, vijay T, et al. Cutting mechanism by giving through Geneva mechanism. *Int J Innov Sci Eng Technol* 2015; 2 (4): 1172–1175.
10. Ujam AJ, Ejeogo G, Onyeneho KC. Development and application of Geneva mechanism for bottle washing. *Am J Eng Res* 2015; 4 (11): 63–73.
11. Zhang E, Wang L. Parametric design and motion analysis of Geneva wheel mechanism based on the UG NX8.5. In: *International Conference on Manufacturing Engineering and Intelligent Materials*, Advances in Engineering, 2017, vol.100, pp.352–356.
12. Sepahpour B. *Kinematic and kinetic analysis of Geneva mechanisms and their applications to synchronization of motion*. PhD Thesis, New Jersey Institute of Technology, 1994.
13. Figliolini G, Rea P, Angeles J. The pure-rolling cam-equivalent of the Geneva mechanism. *Mech Mach Theory* 2006; 41 (11): 1320–1335.
14. Shaohua S, Jifei C. Kinematic analysis on series combined mechanism of elliptic gear and outer Geneva. *Appl Mech Mater* 2013; 312: 42–46.
15. Dijksman EA. Jerk-free Geneva wheel driving. *J Mech* 1966; 1 (3–4): 235–280.
16. Bagci C. Synthesis of double-crank driven mechanisms with adjustable motion and dwell time ratios. *Mech Mach Theory* 1977; 12 (6): 619–638.
17. Yang AT, Hsia LM. Multistage geared Geneva mechanism. *Trans ASME J Mech Des* 1979; 101 (1): 41–46.
18. Fenton RG. Geneva mechanisms connected in series. *Trans ASME J Manuf Sci Eng* 1975; 97: 603–608.
19. Al-Sabeeh AK. Double crank external Geneva mechanism. *Trans ASME J Mech Des* 1993; 115: 666–670.
20. Figliolini G, Rea P. Effects of the design parameters on the synthesis of Geneva mechanisms. *Proc Inst Mech Eng C J Mech Eng Sci* 2012; 227 (9): 2000–2009.
21. Yang AT, Hsia LM. Multistage geared Geneva mechanism. *Trans ASME J Mech Des* 1979; 101: 41–46.
22. Sujan VA, Meggiolaro MA. Dynamic optimization of Geneva mechanisms. In: *International Conference on Gearing, Transmissions and Mechanical Systems*, 2000, pp.687–696.
23. Sadek KSH., Lloyd JL, Smith MR. A new design of Geneva drive to reduce shock loading. *Mech Mach Theory* 1990; 25: 589–595.
24. Cheng CY, Lin Y. Improving dynamic performance of the Geneva mechanism using non-linear spring elements. *Mech Mach Theory* 1995; 30: 119–129.
25. Fenton RG, Zhang Y, Xu J. Development of a new Geneva mechanism with improved kinematic characteristics. *Trans ASME J Mech Des* 1991; 113 (1): 40–45.
26. Lee HP. Design of a Geneva mechanism with curved slots using parametric polynomials. *Mech Mach Theory* 1998; 33 (3): 321–329.
27. Lee JJ, Huang KF. Geometry analysis and optimal design of Geneva mechanisms with curved slots. *Proc Inst Mech Eng C J Mech Eng Sci* 2004; 218 (4): 449–458.

28. Lee JJ, Jan BH. Design of Geneva mechanisms with curved slots for non-undercutting manufacturing. *Mech Mach Theory* 2009; 44 (6): 1192–1200.
29. Li HT. Design of a new kind of curved groove on Geneva mechanism. *J China Agric Univ* 2005; 10: 62–65.
30. DuMont CL, Kurtz AF, Silverstein BD, et al. Design improvement for motion picture film projectors. In: *143rd Technical Conference and Exhibition*, New York, 2001, pp.785–791.
31. Zhang J, Sun S, Tuan HA. Optimization design and analysis of rotary indexing mechanism of tool magazine in machining center. *Jordan J Mech Ind Eng* 2020; 14 (1): 1–6.
32. Heidari M, Atai AA, Shariat Panahi M. An improved Geneva mechanism for optimal kinematic performance. *Proc Inst Mech Eng C J Mech Eng Sci* 2012; 226 (6): 1515–1525.
33. Polyudov OM. *Mechanics of printing machines.* Kyiv: NMKVO, 1991.
34. Uicker JJ, Pennock GR, Shigley JE. *Theory of machines and mechanisms*. 5th ed. New York: Oxford University Press, 2017.

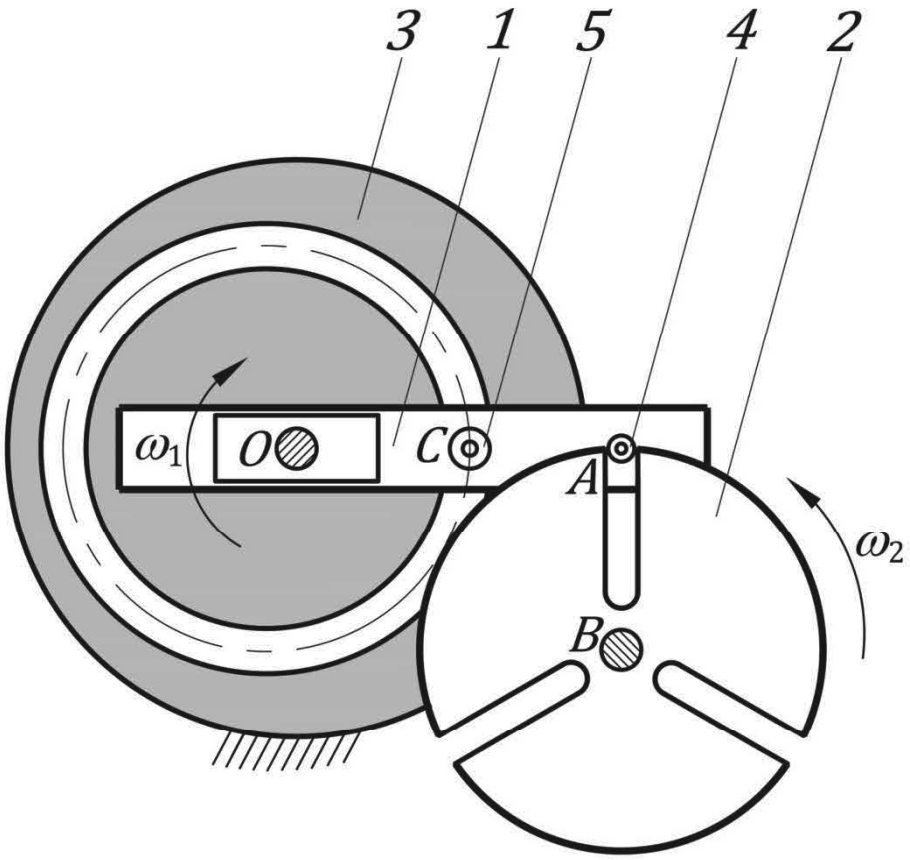

Figure 1. General schematic of the groove cam Geneva mechanism: input crank 1, output wheel 2, groove cam 3, driving pin 4 and roller follower 5

80x80mm (600 x 600 DPI)

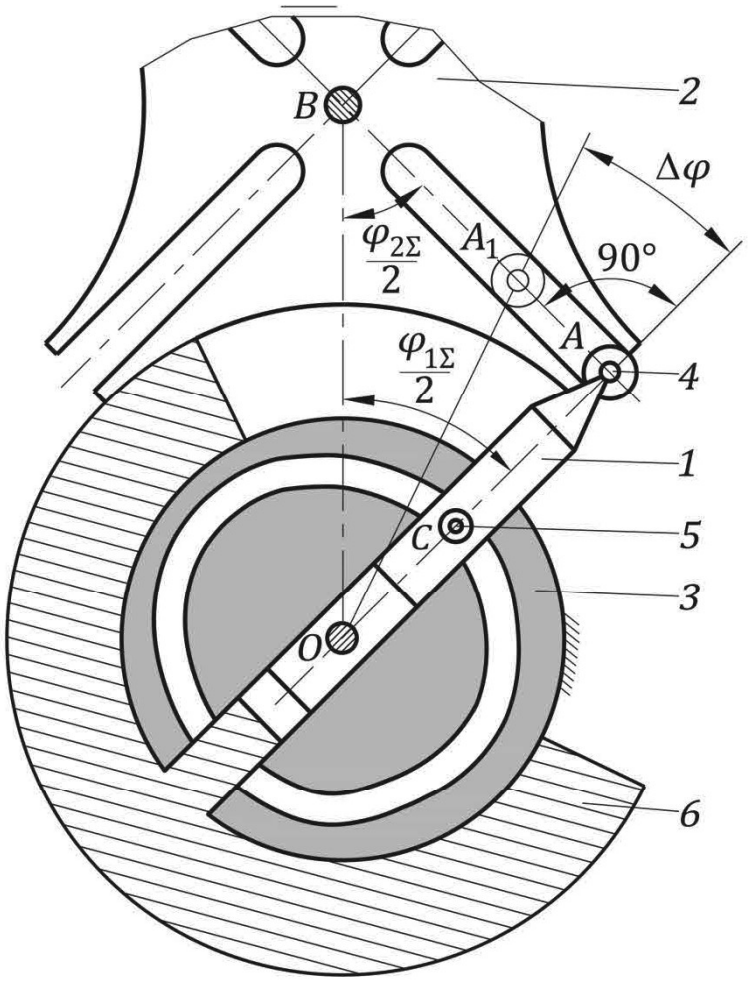

Figure 2. Detailed schematic of the groove cam Geneva mechanism: input crank 1, output wheel 2, groove cam 3, driving pin 4 and roller follower 5, locking ring 6

119x119mm (600 x 600 DPI)

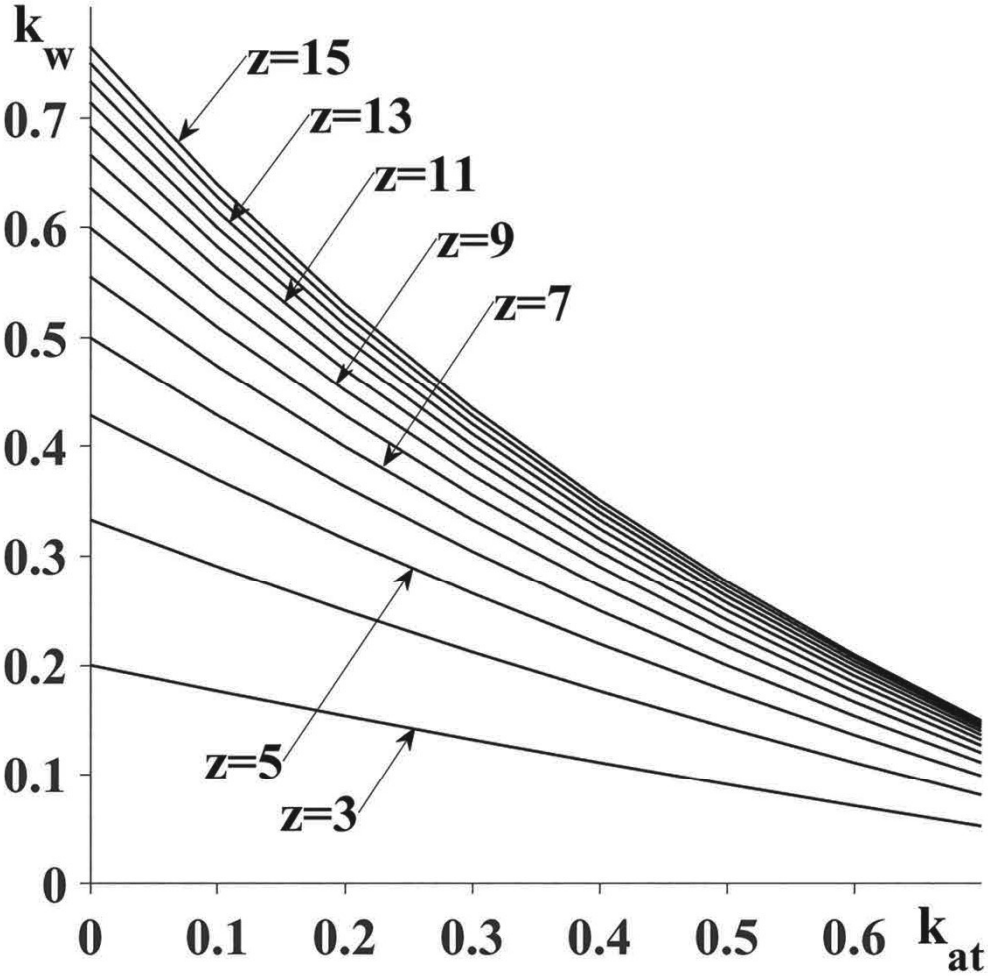

Figure 3. Dependence of the operating time coefficient k_w on the additional dwell coefficient k_{at} and number z of slots

80x80mm (600 x 600 DPI)

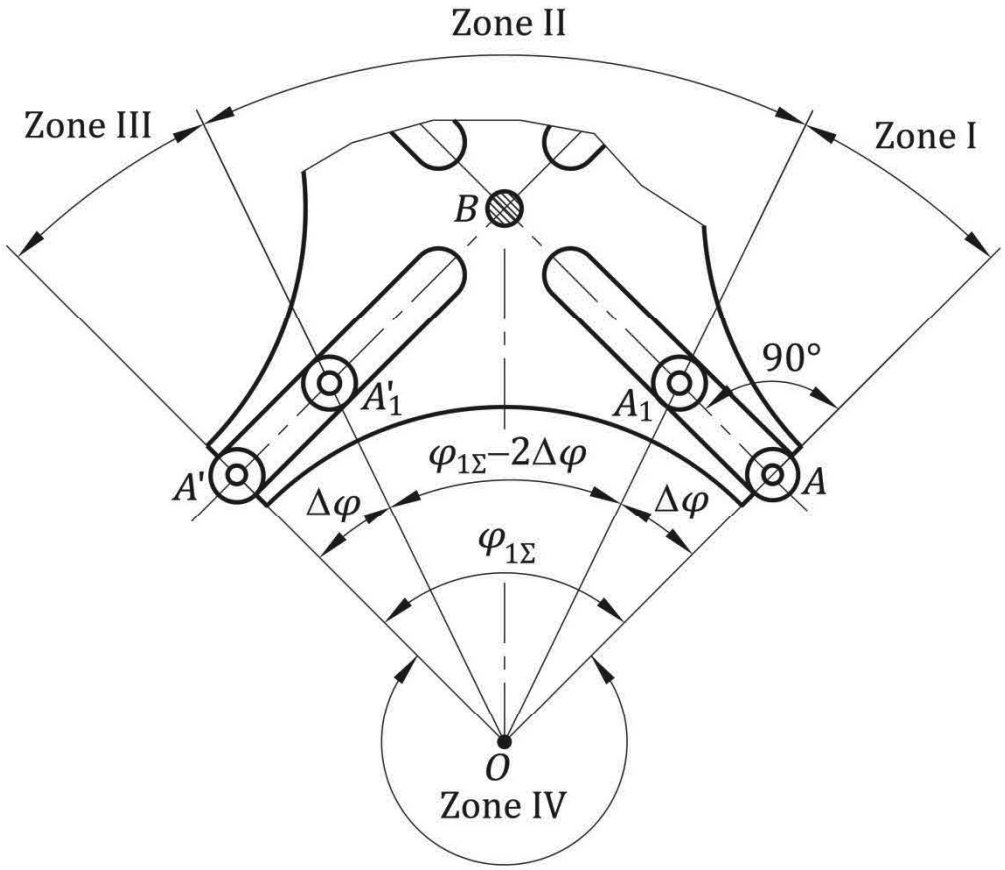

Figure 4. Characteristic zones of the crank rotation

119x119mm (600 x 600 DPI)

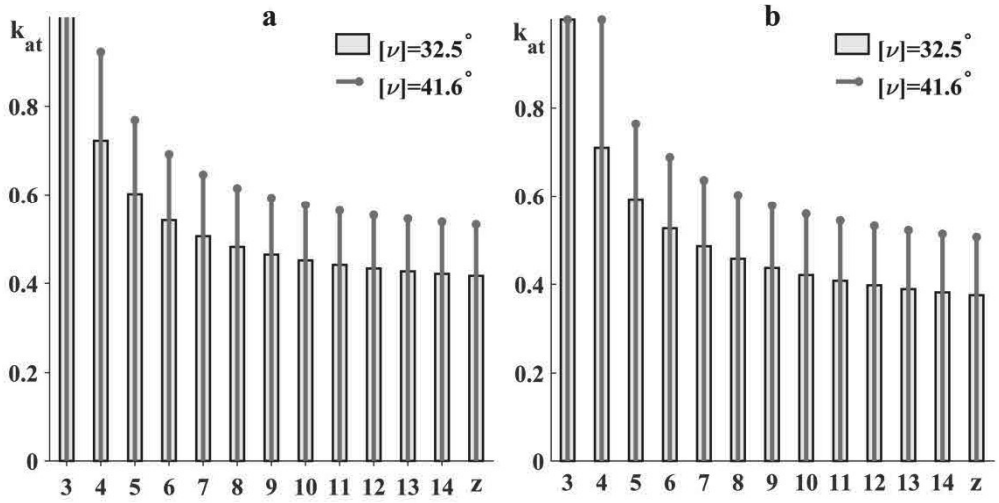

Figure 5. Range of the additional dwell coefficient k_{at} depending on the number z of slots: (a) zone I; (b) zone II

159x80mm (600 x 600 DPI)

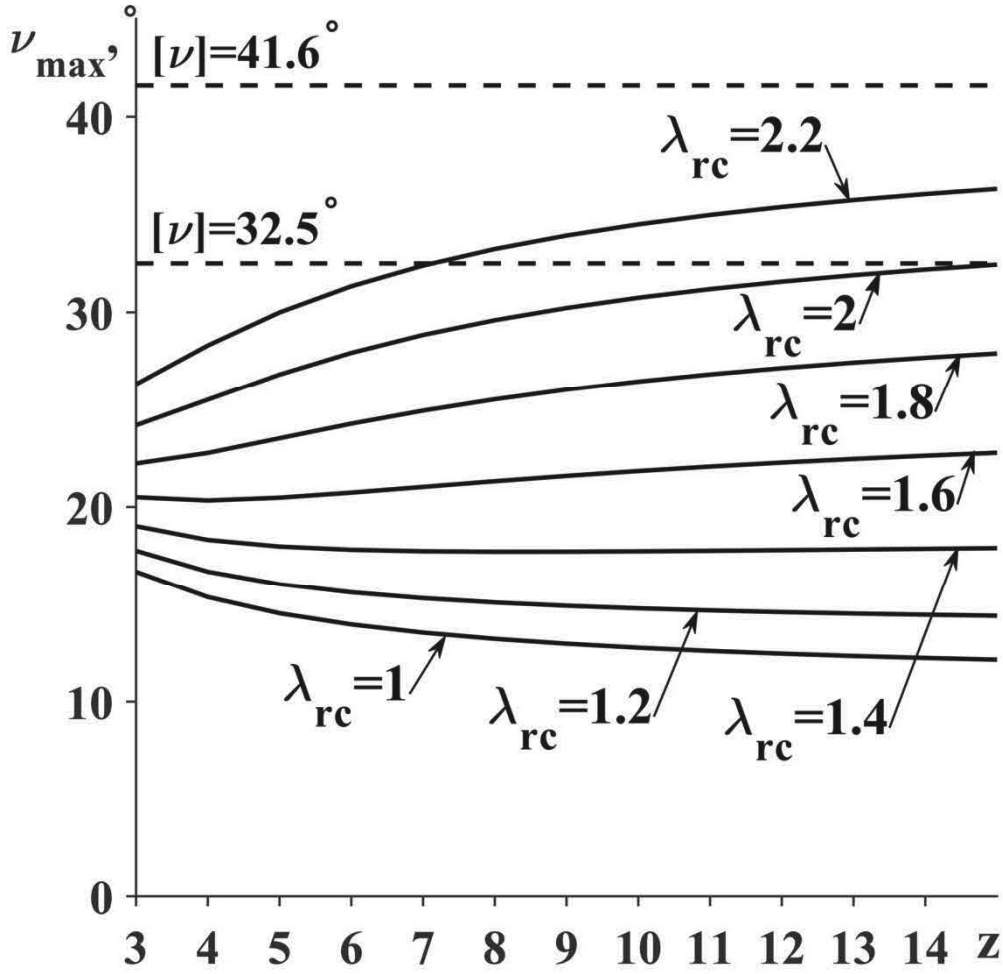

Figure 6. Dependence of the maximum pressure angle ν_{max} on the number z of slots and limiting radius λ_{rc} in the zone IV

80x80mm (600 x 600 DPI)

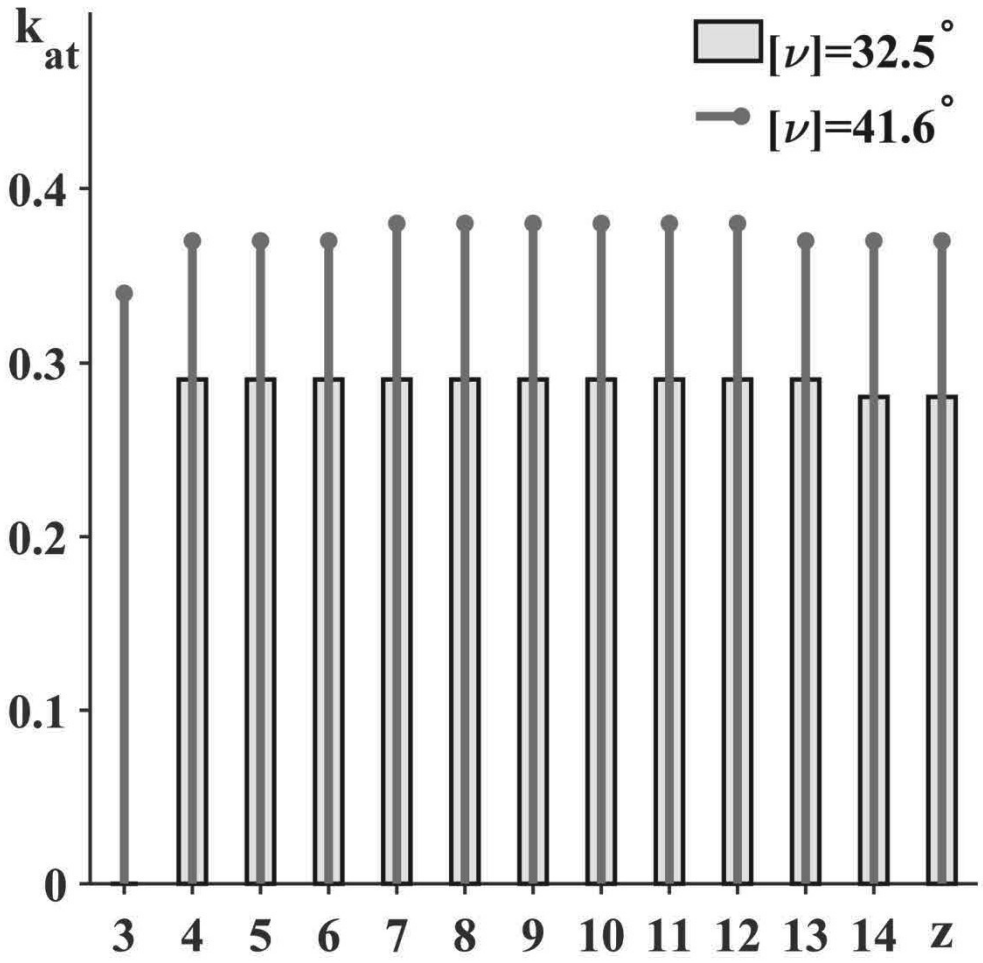

Figure 7. Range of the additional dwell coefficient k_{at} depending on the number z of slots in the zone II

80x80mm (600 x 600 DPI)

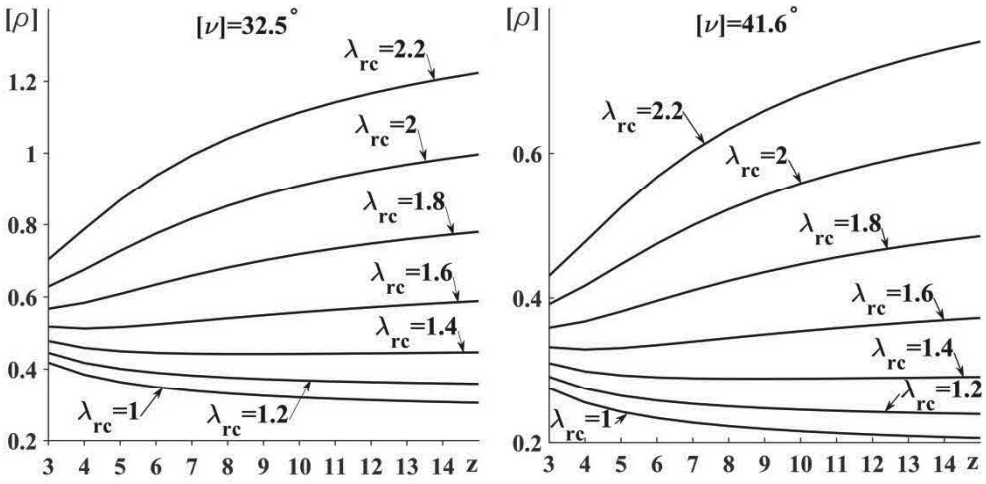

Figure 8. Dependence of the allowable curvature radius [ρ] of the cam profile on the number z of slots and limiting radius λ_{rc} in the zone IV

159x80mm (600 x 600 DPI)

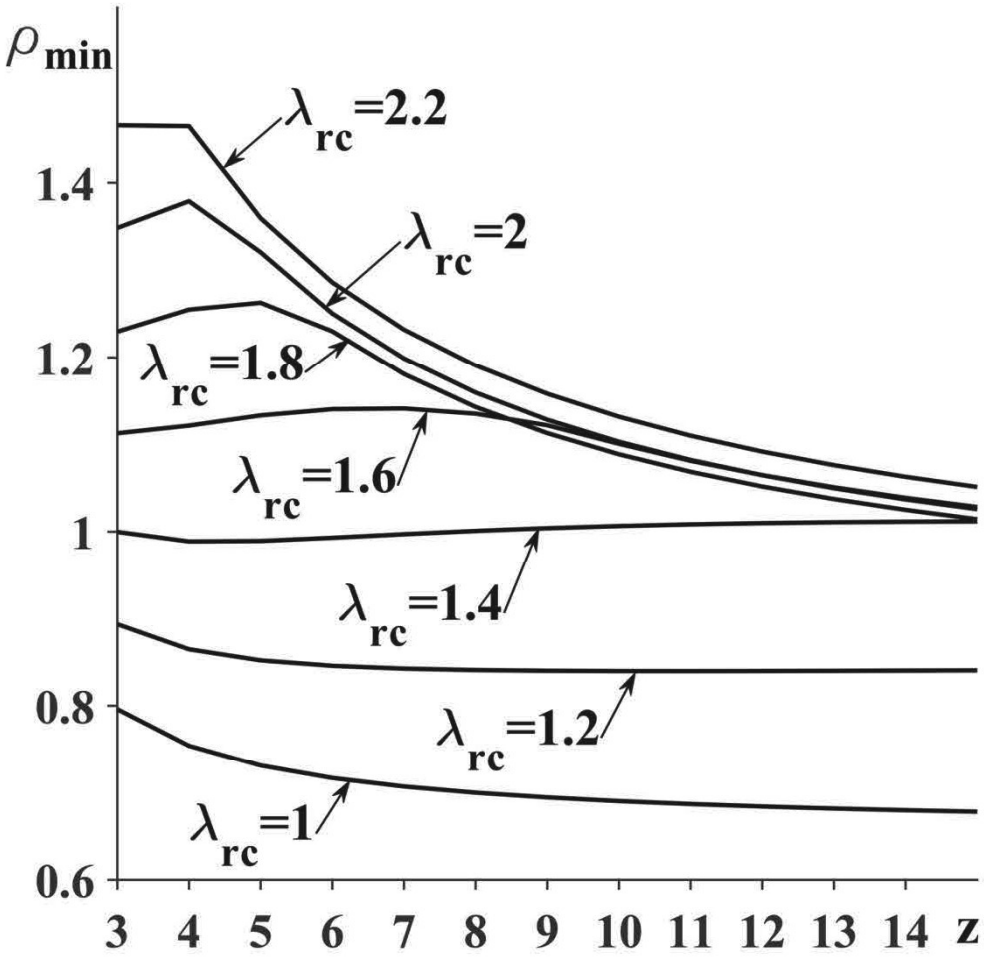

Figure 9. Dependence of the minimum curvature radius ρ_{min} of the cam profile on the number z of slots and limiting radius λ_{rc} in the zone IV

80x80mm (600 x 600 DPI)

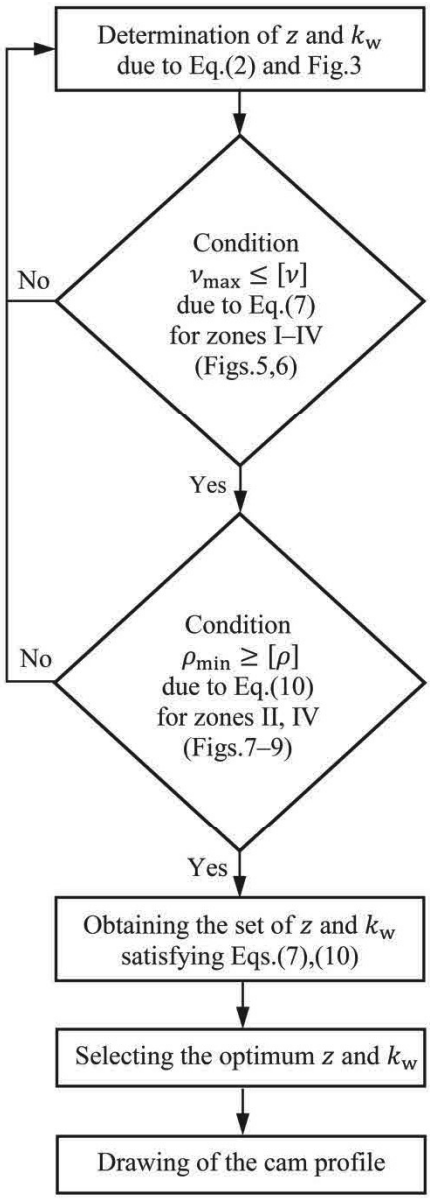

Figure 10. Synthesis algorithm for the groove cam Geneva mechanism

80x199mm (600 x 600 DPI)

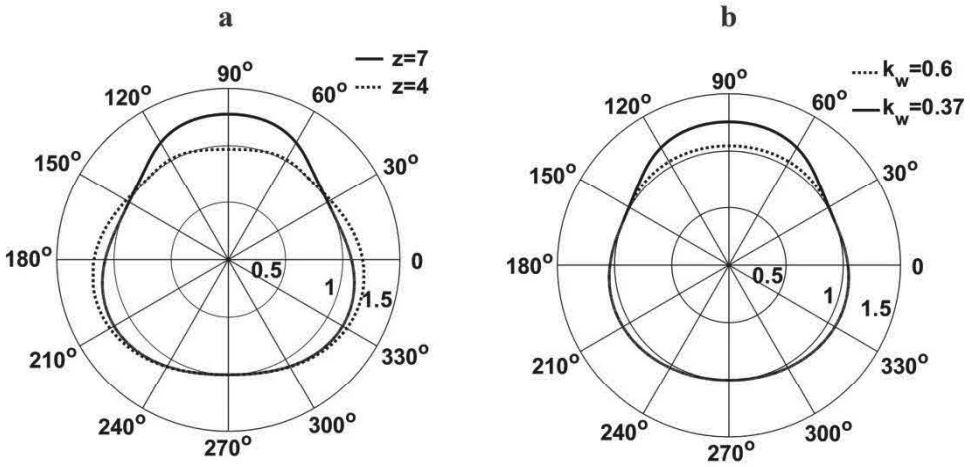

Figure 11. Synthesised paths of the driving pin: (a) k_w=0.3; (b) z=8

159x80mm (600 x 600 DPI)